



저작자표시-비영리-변경금지 2.0 대한민국

이용자는 아래의 조건을 따르는 경우에 한하여 자유롭게

- 이 저작물을 복제, 배포, 전송, 전시, 공연 및 방송할 수 있습니다.

다음과 같은 조건을 따라야 합니다:



저작자표시. 귀하는 원저작자를 표시하여야 합니다.



비영리. 귀하는 이 저작물을 영리 목적으로 이용할 수 없습니다.



변경금지. 귀하는 이 저작물을 개작, 변형 또는 가공할 수 없습니다.

- 귀하는, 이 저작물의 재이용이나 배포의 경우, 이 저작물에 적용된 이용허락조건을 명확하게 나타내어야 합니다.
- 저작권자로부터 별도의 허가를 받으면 이러한 조건들은 적용되지 않습니다.

저작권법에 따른 이용자의 권리는 위의 내용에 의하여 영향을 받지 않습니다.

이것은 [이용허락규약\(Legal Code\)](#)을 이해하기 쉽게 요약한 것입니다.

[Disclaimer](#)

**Study on multifunctional phosphite-based
additives to improve electrochemical properties of
 $\text{LiNi}_{0.5}\text{Mn}_{1.5}\text{O}_4$ cathodes in lithium ion batteries**

Young-Min Song

Department of Energy Engineering
(Battery Science and Technology)
Graduate School of UNIST

**Study on multifunctional phosphite-based
additives to improve electrochemical properties of
 $\text{LiNi}_{0.5}\text{Mn}_{1.5}\text{O}_4$ cathodes in lithium ion batteries**

A thesis

submitted to the Graduate School of UNIST

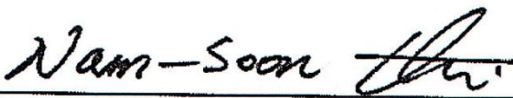
in partial fulfillment of the
requirements for the degree of

Master of Science

Young-Min Song

06.05.2015 of submission

Approved by



Major Advisor

Nam-Soon Choi

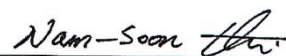
**Study on multifunctional phosphite-based
additives to improve electrochemical properties of
 $\text{LiNi}_{0.5}\text{Mn}_{1.5}\text{O}_4$ cathodes in lithium ion batteries**

Young-Min Song

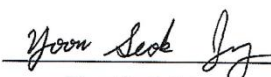
This certifies that the thesis of Young-Min Song is approved.

06.05.2015 of submission

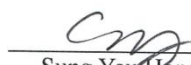
signature


Thesis supervisor: Nam-Soon Choi

signature


YoonSeok Jung

signature


Sung You Hong

Abstract

Nowadays, lithium ion batteries (LIBs) are one of the fastest growing fields as substitute resources due to relative long term cycle and higher energy density than other batteries. Although LIBs have been commercialized in our life, desire values for extensive applications, which require higher energy/power density such as electric vehicle (EV), hybrid electric vehicle (HEV), plug-in hybrid electric vehicle (PHEV), military and aerospace applications, stationary energy storage still remained challenging.

To overcome the limited energy density of LIBs, $\text{LiNi}_{0.5}\text{Mn}_{1.5}\text{O}_4$, which operates in the vicinity of 4.7 V vs. Li/Li^+ , has been considered as a promising cathode material for LIBs due to high energy densities, low cost, eco-friendly and its high specific capacity. However, there are some defects regarding poor cycle performance in full cell at elevated temperature, severe decomposition of solvent and salt, transition metal dissolution, weakness of storage capacity (self-discharge), and so on.

Herein, to resolve the problems of high-voltage $\text{LiNi}_{0.5}\text{Mn}_{1.5}\text{O}_4$ cathode, various organo phosphorus-based additives are investigated as a functional additive forming the solid electrolyte interphase (SEI) layer on the cathode surface. Because this protective layer has less resistive character, it can remain to high capacity at high current rate, moreover, indicate superior cycling performance at elevated temperatures in $\text{Li}/\text{LiNi}_{0.5}\text{Mn}_{1.5}\text{O}_4$ half cell and graphite/ $\text{LiNi}_{0.5}\text{Mn}_{1.5}\text{O}_4$ full cell. To understand the effect of TMSP on the transition metal dissolution, inductively coupled plasma-mass spectrometer (ICP/MS) and energy-dispersive X-ray spectroscopy (EDS) are used as instruments. The results show TMSP-added electrolytes reduce dissolution of Mn and Ni from $\text{LiNi}_{0.5}\text{Mn}_{1.5}\text{O}_4$ cathode.

To check structure stability and ability to protect self-discharge at high temperatures, the fully charged cells are stored at 60 °C, and then the samples are transported to ex-situ X-Ray diffraction (XRD), and the data reveals TMSP-derived SEI layer keeps their nature charged structure which means protect self-discharge during storing at 60 °C.

Another functional effect is to diminish HF produced by hydrolysis of LiPF_6 due to water trace in the cell via ^{19}F and ^{31}P NMR spectra of the electrolyte with and without 0.5wt% TMSP after hydrolysis tests at room temperature. By reducing HF, transition metal dissolution from $\text{LiNi}_{0.5}\text{Mn}_{1.5}\text{O}_4$ cathode by directly attack can be mitigated and protect persistent decomposition of salts.

Also, to confirm the critical impact and additional function of organo phosphorus-based additives, we introduce progressive study comparing TMSP with other additives commonly retaining phosphite core. In addition, from an analysis of surface chemistry of SEI layers on the high voltage cathode, we can find similar components of SEI layers formed by various phosphite-added electrolytes via ex-situ

X-ray photoelectron spectroscopy (XPS), and propose its common functions which eliminate HF and alleviate decomposition of LiPF_6 by hydrolysis via nuclear magnetic resonance (NMR). To understand the effect of various phosphite-types additives regarding self-discharge, open circuit voltage (OCV) of the cells with and without additives is measured at high temperatures during 6 days and capacity retention is conducted after storage.

To sum up, there are lots of additives to improve performance of lithium ion battery, TMSP is one of promising additive to make organic and inorganic based SEI layer on the $\text{LiNi}_{0.5}\text{Mn}_{1.5}\text{O}_4$ cathode and show superior electrochemical performance.

Contents

CHAPTER I.....	11
1.1. Introduction	11
1.1.1 Lithium ion batteries (LIBs).....	11
1.1.2 Spinel Lithium nickel manganese oxide (Spinel $\text{LiNi}_{0.5}\text{Mn}_{1.5}\text{O}_4$).....	13
1.1.2-1 Crystal structure of $\text{LiNi}_{0.5}\text{Mn}_{1.5}\text{O}_4$	13
1.1.2-2 Problems of $\text{LiNi}_{0.5}\text{Mn}_{1.5}\text{O}_4$	15
1.1.3 Strategies to stable high-voltage $\text{LiNi}_{0.5}\text{Mn}_{1.5}\text{O}_4$ cathode.....	17
1.2. Backgrounds of my research.....	19
1.2.1 Electrolyte.....	19
1.2.2 SEI layer.....	21
1.3.2 Electrolyte additive.....	22
 CHAPTER II. The promising candidate as functional additive for $\text{LiNi}_{0.5}\text{Mn}_{1.5}\text{O}_4$ cathodes with superior electrochemical performance.....	 24
2.1 Introduction.....	24
2.2 Experimental.....	27
2.2.1 Electrolyte and electrode preparation.....	27
2.2.2 Electrochemical Measurements.....	27
2.2.3. Characterization.....	28
2.3 Result and discussion.....	29
2.3.1 Improved electrochemical performance by using TMSP additive.....	28
2.3.2 Comparison with phosphite-based additives.....	52
2.4 Conclusion.....	65
 References.....	 66

List of figures

Fig. 1-1 A conventional lithium-ion battery contains a graphite anode, a lithium cathode, and a liquid electrolyte containing lithium ions in a separator.

Fig. 1-2 Basic LIB characteristics required for different application.

Fig. 1-3 Crystal structures of $\text{LiNi}_{0.5}\text{Mn}_{1.5}\text{O}_4$ with disordered and ordered structures.

Fig. 1-4 The differences between disordered and ordered $\text{LiNi}_{0.5}\text{Mn}_{1.5}\text{O}_4$. (a) Representative X-ray patterns of ordered and disordered $\text{LiNi}_{0.5}\text{Mn}_{1.5}\text{O}_4$ spinel samples. (b) Typical electrochemical charge and discharge profiles of ordered and disordered $\text{LiNi}_{0.5}\text{Mn}_{1.5}\text{O}_4$ spinel cathodes.

Fig. 1-5 The representation of electrochemical stability window of conventional electrolytes.

Fig. 1-6 Schematic illustration described reasons of capacity fading of $\text{LiNi}_{0.5}\text{Mn}_{1.5}\text{O}_4$ cathode.

Fig. 1-7 Procedure of HF generation by hydrolysis of LiPF_6 salts.

Fig. 1-8 Strategies to stable high-voltage $\text{LiNi}_{0.5}\text{Mn}_{1.5}\text{O}_4$ cathode. (1) Add additive for stable solid electrolyte interphase (SEI) layer, (2) Replace solvent for high anodic stability.

Fig. 1-9 Comparison of molecular structures and computed Oxidation Potential (V_{ox}).

Fig. 1-10 Molecular structure of typical cyclic and linear carbonates.

Fig. 1-11 Properties of organic solvents.

Fig. 1-12 Presentation of SEI lay and process of growth as cycle goes on.

Fig. 1-13 Molecular orbital energies of additive and carbonate-based electrolyte and electron movement according to their molecular orbital energies.

Fig. 2-1 Schematic representation of the different secondary batteries in terms of power density and energy density.

Fig. 2-2 Strategies to increase energy density of LIB.

Fig. 2-3 Oxidation stability and ionic conductivity of desirable high voltage solvent-based electrolytes.

Fig. 2-4 The calculated highest occupied molecular orbital (HOMO) and lowest unoccupied molecular orbital (LUMO) energy levels of TMSP, VC, FEC additives and an EC solvent. The HOMO is situated at the electron-rich moieties showing the donor character.

Fig. 2-5 Electrochemical performance of $\text{LiNi}_{0.5}\text{Mn}_{1.5}\text{O}_4$ cathodes: (a) cycling stability when cycled between 3.5 and 5.0 V at a rate of C/2, (b) rate capability at different C rates, (c) charge and discharge curves at a rate of C/2, and (d) charge and discharge curves at a rate of 3 C.

Fig. 2-6 XRD patterns of fully charged $\text{Li}_x\text{Ni}_{0.5}\text{Mn}_{1.5}\text{O}_4$ cathode before and after stored at 60 °C for 1day. The XRD pattern of fresh $\text{LiNi}_{0.5}\text{Mn}_{1.5}\text{O}_4$ cathode is displayed for comparison. The XRD data reveals that a fully charged cathode stored in the TMSP-added electrolyte at 60 °C experiences less re-lithiation (self-discharge).

Fig. 2-7 Comparison of cycling stability of $\text{LiNi}_{0.5}\text{Mn}_{1.5}\text{O}_4$ cathodes with various electrolytes at 60 °C at a current density of 60 mA g⁻¹.

Fig. 2-8 (a) Discharge capacity, (b) Coulombic efficiency of the $\text{LiNi}_{0.5}\text{Mn}_{1.5}\text{O}_4$ cathodes in baseline and TMSP-added electrolytes at 30 °C at a current density of 60 mA g⁻¹.

Fig. 2-9 EIS spectra for $\text{LiNi}_{0.5}\text{Mn}_{1.5}\text{O}_4$ cathodes precycled in baseline or 0.5% TMSP-added electrolyte.

Fig. 2-10 F 1s and P 2p XPS spectra of the $\text{LiNi}_{0.5}\text{Mn}_{1.5}\text{O}_4$ cathodes after precycling at 30 °C and 5 cycles at 60 °C.

Fig. 2-11 Schematic representation of possible mechanisms for electrochemical oxidative decomposition of TMSP and unique function of TMSP scavenging HF from the electrolyte. The products produced by TMSP decomposition will contribute to the formation of the SEI on the $\text{LiNi}_{0.5}\text{Mn}_{1.5}\text{O}_4$ cathode.

Fig. 2-12 XPS spectra of the $\text{LiNi}_{0.5}\text{Mn}_{1.5}\text{O}_4$ cathodes cycled in TMSP-added electrolyte.

Fig. 2-13 ¹⁹F and ³¹P NMR spectra of the electrolyte with and without 0.5wt% TMSP after hydrolysis tests at room temperature. HF was completely removed from the electrolyte in presence of TMSP.

Fig. 2-14 O 1s XPS spectra of the $\text{LiNi}_{0.5}\text{Mn}_{1.5}\text{O}_4$ cathodes before and after 5 cycles in the baseline and TMSP-added electrolytes at 60 °C.

Fig. 2-15 Electrochemical performance of graphite/ $\text{LiNi}_{0.5}\text{Mn}_{1.5}\text{O}_4$ full cells at C/2 and 30 °C when cycled between 3.0 and 5.0 V: (a) cycling stability and (b) coulombic efficiency, charge and discharge curves of the full cell for 1st, 30th, 50th, 80th and 100th cycles in (c) baseline electrolyte and (d) TMSP-added electrolyte. A very high coulombic efficiency (red square) of over 99.5%, which is vital for practical applications, was obtained.

Fig. 2-16 Voltage profiles of the graphite anode with or without 0.5% TMSP for a current density of 35 mA g⁻¹ (electrode capacity = 2.55 mAh cm⁻²) during precycling.

Fig. 2-17 (a) Discharge capacity, (b) Coulombic efficiency of graphite/ $\text{LiNi}_{0.5}\text{Mn}_{1.5}\text{O}_4$ full cells in baseline and TMSP-added electrolytes at 45 °C at a rate of C/2.

Fig. 2-18 EDS patterns and SEM images of (a) pristine graphite and graphite anodes retrieved from graphite/ $\text{LiNi}_{0.5}\text{Mn}_{1.5}\text{O}_4$ full cells after 100 cycles at 30 °C in (b) baseline electrolyte and (c) TMSP-added electrolyte. Scale bar represents 5 μm. (d) ICP result showing the amount of Mn and Ni dissolution from non-cycled $\text{LiNi}_{0.5}\text{Mn}_{1.5}\text{O}_4$ cathodes in the electrolytes with and without TMSP at 60 °C for 12 h. The use of TMSP inhibited the Mn and Ni dissolution from the pristine cathode. (e) Schematic illustration of unique functions of TMSP in a full cell.

Fig. 2-19 (a) Initial charge and discharge profiles at 30 °C and (b) dQ/dV graphs of 5 V-class $\text{LiNi}_{0.5}\text{Mn}_{1.5}\text{O}_4$ cathodes in various electrolytes during 5 cycles at 60 °C after initial cycling at 30 °C.

Fig. 2-20 FE-SEM images of the $\text{LiNi}_{0.5}\text{Mn}_{1.5}\text{O}_4$ cathodes after 5 cycles at 60 °C: (a) pristine cathode,

(b) baseline electrolyte, (c) 1% VC-added, (d) 5% FEC-added, and (e) 0.5% TMSPadded.

Fig. 2-21 O 1s and C 1s XPS spectra of the $\text{LiNi}_{0.5}\text{Mn}_{1.5}\text{O}_4$ cathodes cycled in baseline and VC-added electrolytes during 5 cycles at 60 °C.

Fig. 2-22 (a) Potentiostatic profiles of Li/ $\text{LiNi}_{0.5}\text{Mn}_{1.5}\text{O}_4$ half cells maintained at charging voltage of 5.0 V after charging up to 5.0 V at 30 °C. (b) Linear sweep voltammetry of electrolytes with and without 0.5% TMSP additive. Stainless steel was used as a working electrode and the scan rate was 1 mV/s.

Fig. 2-23 Molecular structures of various phosphite-containing additives.

Fig. 2-24 The voltage profiles of $\text{LiNi}_{0.5}\text{Mn}_{1.5}\text{O}_4/\text{Li}$ cell in EC/EMC/DMC 1.0M LiPF_6 without and with 0.5wt% additive.

Fig. 2-25 (a) Potentiostatic profiles of $\text{LiNi}_{0.5}\text{Mn}_{1.5}\text{O}_4/\text{Li}$ half cells maintained at charging voltage of 5.0V after charged up to 5.0V at 30 °C, (b) charge and discharge curves by galvanostatic intermittent titration technique (GITT)

Fig. 2-26 Electrochemical performance of $\text{LiNi}_{0.5}\text{Mn}_{1.5}\text{O}_4$ cathodes at C/2 when cycled between 3.5 and 5.0V: (a) Cycling stability at 30 °C and (b) coulombic efficiency at 30 °C. (c) Cycling stability at 60 °C and (d) coulombic efficiency at 60 °C.

Fig. 2-27 XPS spectra of the $\text{LiNi}_{0.5}\text{Mn}_{1.5}\text{O}_4$ cathodes after precycling at 30 °C.

Fig. 2-28 ^{19}F NMR spectra of the electrolyte with and without additive after hydrolysis tests at room temperature. HF was completely removed from the electrolyte in presence of phosphite-containing additives.

Fig. 2-29 ^{31}P NMR spectra of the electrolyte with and without additive after hydrolysis tests at room temperature.

Fig. 2-30 Rate capability at different C rates depending on additive.

Fig. 2-31 AC impedance spectra of $\text{LiNi}_{0.5}\text{Mn}_{1.5}\text{O}_4$ after precycle in electrolyte with and without additives.

Fig. 2-32 Properties in storage test at 60 °C: (a) representation of OVC drop of Li/ $\text{LiNi}_{0.5}\text{Mn}_{1.5}\text{O}_4$ half-cell, (b) discharge capacity retention after storage during 6 days.

CHAPTER I.

1.1 Introduction

1.1.1 Lithium ion batteries (LIBs)

To substitute current exhausted energy sources, lots of batteries such as primary battery, solar cell, fuel cell, secondary battery, have been researched. Lithium ion battery (LIB) is one of promising candidate due to relative high energy density.²

Lithium ion batteries include a positive electrode (LiCoO_2) having current collector (aluminum foil) and a negative electrode (carbonaceous material such as graphite) having current collector (copper foil) and non-aqueous liquid electrolyte (carbonate-base electrolyte), and separator (materials properly mixed polyethylene (PE) and polypropylene (PP)). The electrolytes enable solvated lithium ions to migration between cathode and anode during charging or discharging process. Separator is a material which protects physical contact by separating a positive electrode from a negative electrode and only transport lithium ion between the electrodes.⁴

The principle of LIBs is that lithium ions move between the positive electrode and the negative electrode during charging and discharging process of the battery. For example, when the battery is charged, the removal of lithium ions by the simultaneous oxidation of cobalt in the cathode and insertion of lithium ions into the graphite anode occurs. Contrast to charging process, when the battery is discharged, lithium ions flow from the negative electrode to the positive electrode (Fig .1-1).

So far, LIBs have been broadly used and applied to energy storage devices such as mobile phone, portable PC, electric vehicle (EV), hybrid electric vehicle (HEV), plug-in hybrid electric vehicle (PHEV), military and aerospace applications, stationary energy storage systems.¹⁻⁵ Although LIBs successfully commercialized as a alternative resource, in order to proper utilize each different systems, it is important to know thier characteristics required for different application showed in Fig. 1-2. Moreover, additional stuties should be conducted in order to achieve progresive result and solve disadvantages which carry out high energy density and capacity.¹

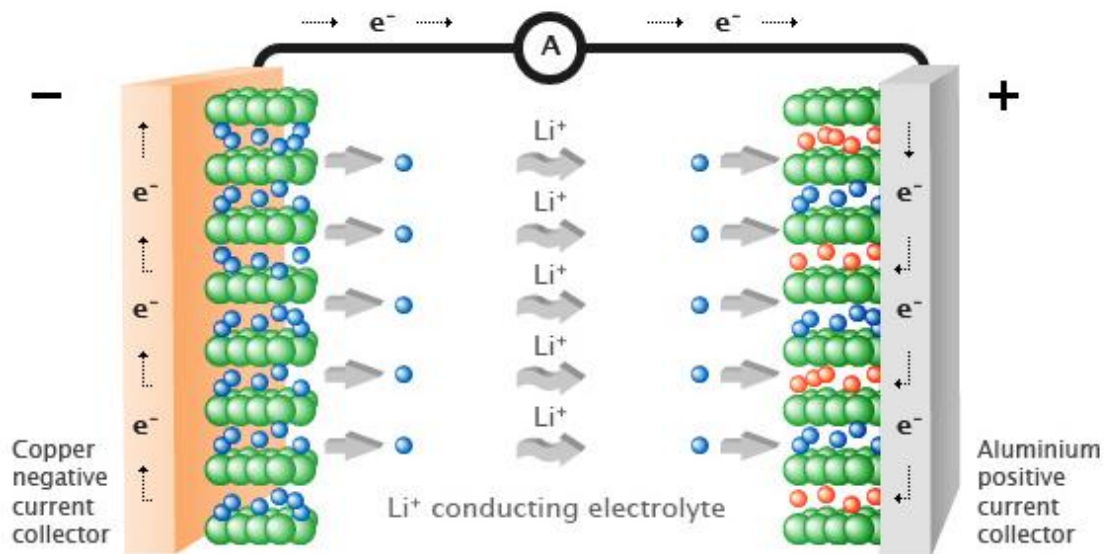


Fig. 1-1 A conventional lithium-ion battery contains a graphite anode, a lithium cathode, and a liquid electrolyte containing lithium ions in a separator.


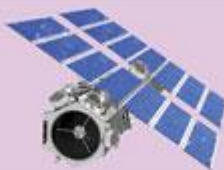


<p align="center">Consumer Electronics</p>  <p>Smart Phone Portable PC Mobile Phone</p> <p>Small LIB with energies <100 Whr</p> <ul style="list-style-type: none"> • High energy density = increase run time • Light weight = increase portability • High power density = faster processor power etc. 	<p align="center">Aerospace Applications</p>  <p>Energy density: 260-310 Whr.L⁻¹; Cycle life: Satellites for Geo-Synchronous earth orbit: 12000-24000 cycles at 60% DOD over a 15 year period, For satellites at Low-earth orbit: 5,000 cycles at 25% DOD over seven years</p> <p>Long-life, high energy densities and lightweight and the prime requirements for aerospace applications</p>
<p align="center">Electric Vehicles</p>  <p>Power density: 660-600 W.L⁻¹ Energy density: C/3 Discharge rate: 230-300 Whr.L⁻¹ Life: 10 years, Cycle life: 1000 to 80%DOD Normal recharge time: to 6 hrs, High rate charge: 40-80% SOC in 15 mins</p> <ul style="list-style-type: none"> • High energy density = Long distance driving • High power density = Excellent driving performance, significant fuel efficiency 	<p align="center">Stationary Energy Storage</p>  <p>Capacity: 2KWh, Energy density: 240 Whr.L⁻¹ Specific energy: 120 Wh.kg⁻¹ Energy efficiency: 90%, Cycle life: 3500 cycles</p> <p>Longer battery lifetime and lower cost are the prime requirements as weight/volume of LIBs are not constrained in immobile applications</p>

Fig. 1-2 Basic LIB characteristics required for different application.

<http://www.nanowerk.com/spotlight/spotid=36096.php>

1.1.2 Spinel Lithium nickel manganese oxide (Spinel $\text{LiNi}_{0.5}\text{Mn}_{1.5}\text{O}_4$)

1.1.2-1 Crystal structure of $\text{LiNi}_{0.5}\text{Mn}_{1.5}\text{O}_4$

Because LIBs have high energy density, it have been adopted to broad applications. To put the practical use, spinel lithium manganese oxide cathode (LiMn_2O_4) has been commercialized in the first generation of hybrid electric vehicle (HEV), plug-in hybrid electric vehicle (PHEV) in terms of cost, cycle life, energy, but it remained mixed success.⁶ The spinel lithium nickel manganese oxide cathode ($\text{LiNi}_{0.5}\text{Mn}_{1.5}\text{O}_4$) has been received enthusiastic attention as alternative cathode owing to higher energy density and specific capacity, and reduced transition metal dissolution than LiMn_2O_4 cathode.^{7,8} Although these attractive reasons make spinel $\text{LiNi}_{0.5}\text{Mn}_{1.5}\text{O}_4$ cathode promising candidate for next generation of high power batteries, utilizing $\text{LiNi}_{0.5}\text{Mn}_{1.5}\text{O}_4$ cathode is limited by some problems.

The structure of spinel $\text{LiNi}_{0.5}\text{Mn}_{1.5}\text{O}_4$ has robust cubic close-packed crystal structure with edge-shared MO_6 (M=Mn or Ni) octahedral (Fig. 1-3). It can be divided into two structures depending on cation ordering.⁸ First, it is consist of the 3:1 ratio of $\text{Mn}^{4+}:\text{Ni}^{2+}$ with a distinct site and result in a space group of $P4_332$ (ordered structure) which can be made by re-annealing at relative lower temperature 700 °C. On the contrary, Ni and Mn are occupied randomly among 16d octahedral site in case of disordered structure ($Fd3m$) which is generally heated to 900 °C during final sintering process.⁹⁻¹⁴

The difference between ordered and disordered structure is remarkably detected by X-Ray diffraction (XRD) or charge and discharge curves (Fig. 1-4), and electrochemical performance is affected by degree of cation ordering.¹⁵ Generally, the rate properties and cycling performance of the disordered $\text{LiNi}_{0.5}\text{Mn}_{1.5}\text{O}_4$ is superior to that of the ordered one due to the considerable increase of Li^+ diffusion coefficient. However, although disordered $\text{LiNi}_{0.5}\text{Mn}_{1.5}\text{O}_4$ shows better performance than ordered one, Mn^{3+} ion produced by loss of oxygen in order to match the charge neutrality may form Mn^{2+} from disproportion reaction and it dissolves into electrolyte and induces remarkable capacity fading at elevated temperature. In addition, there are many factors influencing characteristics of the cell performance such as particle size and morphology, cation doping, surface modification, electrolyte interaction. Even though the performance of $\text{LiNi}_{0.5}\text{Mn}_{1.5}\text{O}_4$ is definitely improved by changing these factors, severe capacity fade is found in full cell configurations when the cathode is coupled with the graphite anode at elevated temperatures.¹⁶

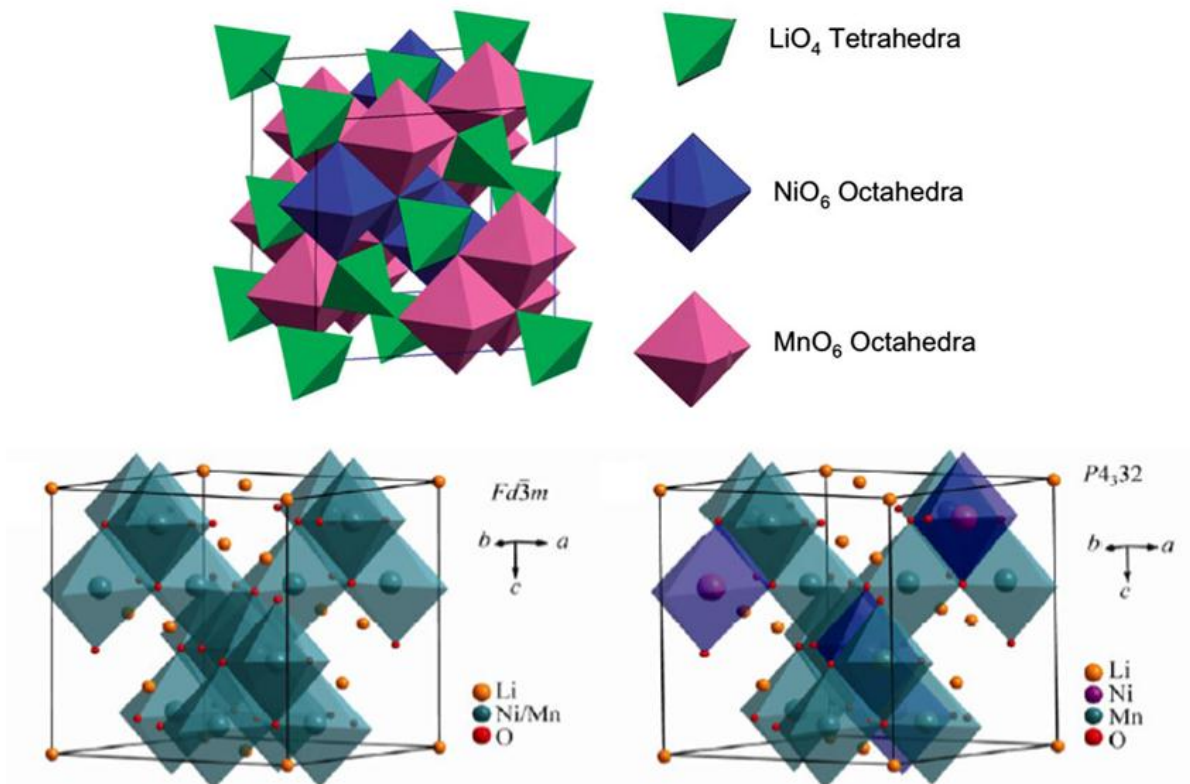


Fig. 1-3 Crystal structures of $\text{LiNi}_{0.5}\text{Mn}_{1.5}\text{O}_4$ with disordered and ordered structures.¹⁵

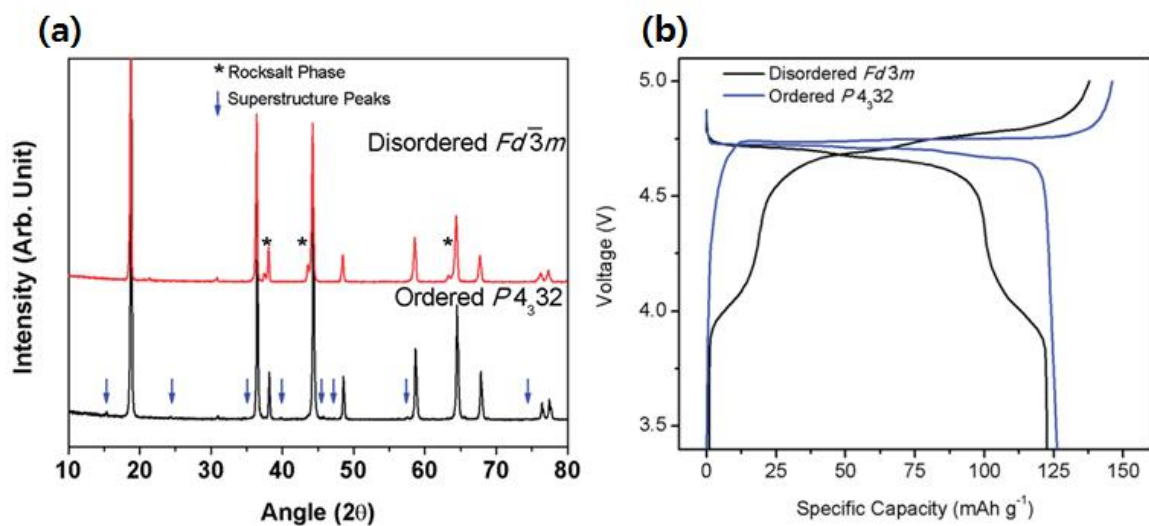


Fig. 1-4 The differences between disordered and ordered $\text{LiNi}_{0.5}\text{Mn}_{1.5}\text{O}_4$. (a) Representative X-ray patterns of ordered and disordered $\text{LiNi}_{0.5}\text{Mn}_{1.5}\text{O}_4$ spinel samples. (b) Typical electrochemical charge and discharge profiles of ordered and disordered $\text{LiNi}_{0.5}\text{Mn}_{1.5}\text{O}_4$ spinel cathodes.¹⁵

1.1.2-2 Problems of of $\text{LiNi}_{0.5}\text{Mn}_{1.5}\text{O}_4$

The defects of high-voltage $\text{LiNi}_{0.5}\text{Mn}_{1.5}\text{O}_4$ cathodes are usually attributed to severe electrolyte decomposition due to high operating potential, transition metal dissolution from cathode, HF generation. Fig. 1-5 indicates electrochemical stability window of conventional electrolytes regarding started potential of oxidative or reductive decomposition. Because oxidative decomposition of solvents and salts occurred approximately over 4.3 V, this can lead to forming thick passivation layer on the surface with consumption of active Li^+ ions, and consequentially impede Li^+ ion diffusion.^{17,18}

When graphite is selected as substitutive Li metal anode, one of the reasons concerning drastic capacity fading is described in Fig. 1-6. Although Mn^{2+} dissolution from disproportionation reaction will be less severe compared to LiMn_2O_4 cathode due to diminished Mn^{3+} ions, it is still critical problem due to high operating voltage. The dissolved Mn^{2+} ions into electrolyte migrates graphite or separator, and are reduced to metallic nanoparticles and blocking lithium pathway.^{19,20}

The reaction regarding hydrolysis between water trace and conventional LiPF_6 salt is described in Fig. 1-7. The resulting product is HF which causes fast capacity fading due to directly attack surface of $\text{LiNi}_{0.5}\text{Mn}_{1.5}\text{O}_4$ cathode and transition metal dissolution. It should be considered to control amount of HF produced by hydrolysis so as to interrupt Ni or Mn dissolution and decomposition of salts.

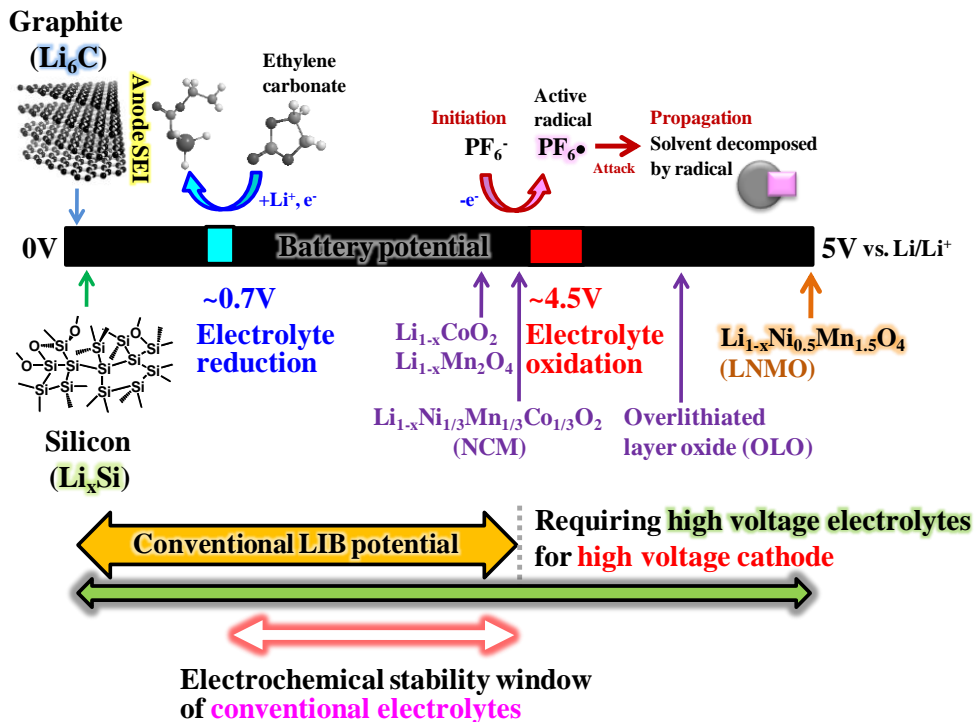


Fig. 1-5 The representation of electrochemical stability window of conventional electrolytes.

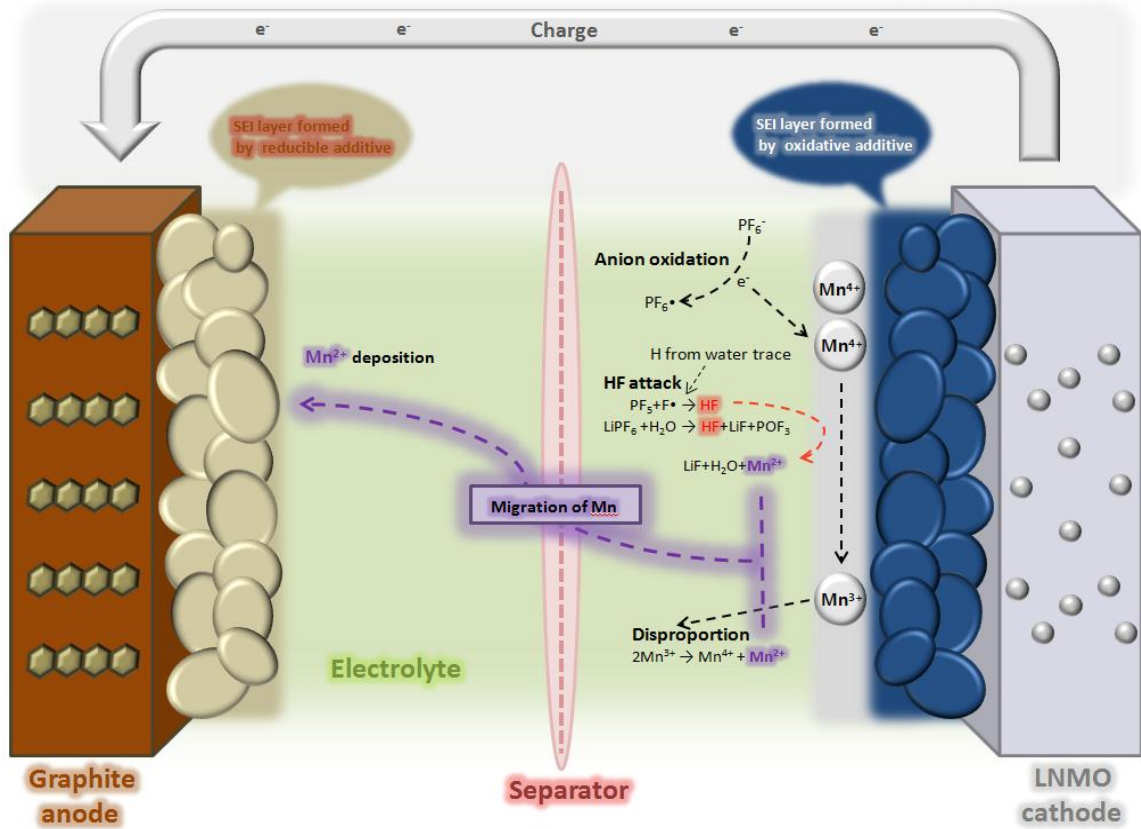


Fig. 1-6 Schematic illustration described reasons of capacity fading of $LiNi_{0.5}Mn_{1.5}O_4$ cathode.

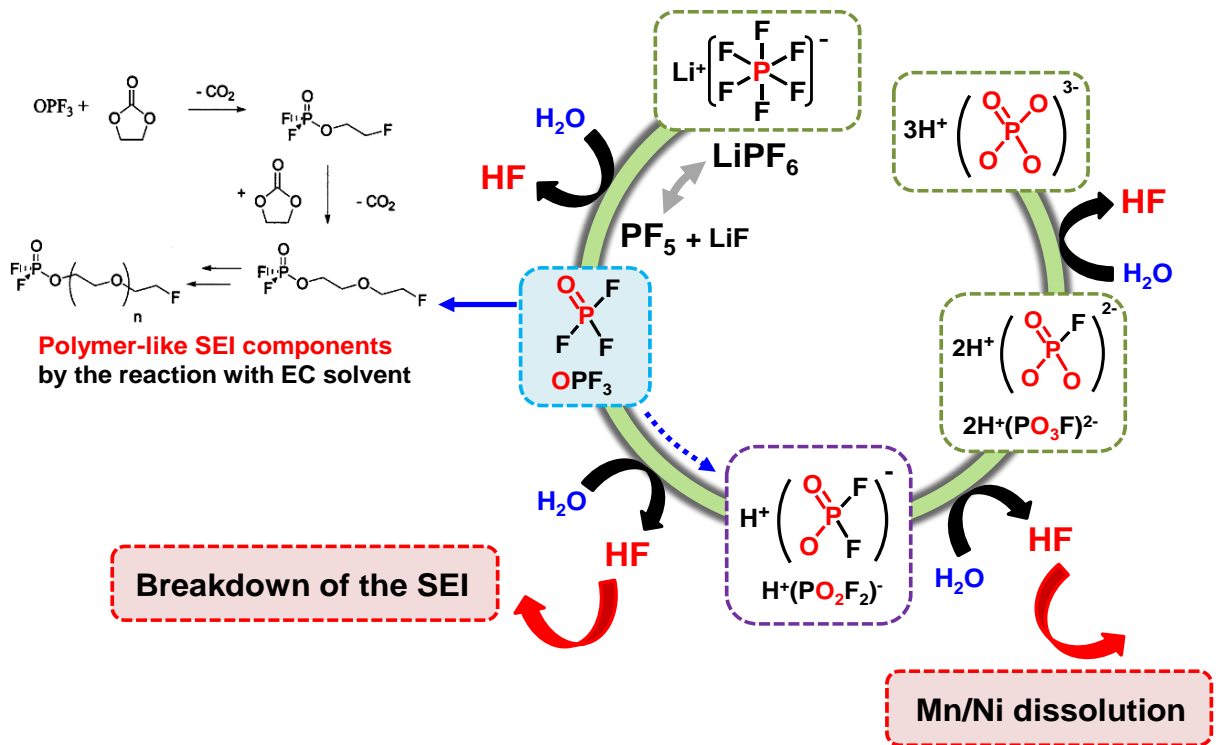


Fig. 1-7 Procedure of HF generation by hydrolysis of $LiPF_6$ salts.

1.1.3 Strategies to stable high-voltage $\text{LiNi}_{0.5}\text{Mn}_{1.5}\text{O}_4$ cathode

One of main reasons of rapid capacity fading when high-voltage $\text{LiNi}_{0.5}\text{Mn}_{1.5}\text{O}_4$ is adopted as cathode regards oxidative decomposition of electrolyte due to relative low oxidation stability of carbonate-base electrolytes.

To protect this problem, generally the strategies have been divided into two perspectives. First, it is forming stable SEI layer on the surface between electrode and electrolytes to alleviate severe decomposition of electrolytes by adding small amount of additive for improved electrochemical performance. Second, it is to replace all or partially commercialized carbonate-base electrolytes with electrolytes which indicate high oxidative stability such as ionic liquid, sulfone, nitrile-base solvents. The discussed approaches are showed in Fig. 1-8, and researches regarding two perspectives are handled more closely.

To stabilize 5 V-class cathode surface, a highly fluorinated phosphate ester additive was investigated. Lithium bis(oxalato)borate (LiBOB) has been known as one of alternative salts of LiPF_6 and additives forming robust SEI layer on Si electrodes as well as graphite anode.^{21,22} Adding LiBOB into electrolytes leads to the formation of passivation film to protect the graphite anode material suffering from exfoliation by the propylenecarbonate-rich electrolyte.²³ Recently, Our group and the Kim group reported the beneficial effects of LiBOB additive with enhanced cycling performance in $\text{LiNi}_{0.5}\text{Mn}_{1.5}\text{O}_4/\text{Li}$ half cell at elevated temperatures.^{24,25}

Sulfone-base electrolytes has high oxidation stability compared to conventional carbonate-base electrolytes, moreover, fluorinated sulfone indicates higher anodic stability than non-fluorinated solvents due to change of electronegativity in molecular structure (Fig. 1-9).²⁶ The similar effects of fluorinated solvents were utilized by the Zhang group to improve the electrochemical performance of $\text{LiNi}_{0.5}\text{Mn}_{1.5}\text{O}_4$ at elevated temperature. The high anodic stability of the fluorinated carbonate solvent-based electrolytes was supported by the electrochemical evaluation results obtained using $\text{LiNi}_{0.5}\text{Mn}_{1.5}\text{O}_4/\text{Li}$ and $\text{LiNi}_{0.5}\text{Mn}_{1.5}\text{O}_4/\text{Li}_4\text{Ti}_5\text{O}_{12}$ electrochemical couples.²⁷

Wang group reported properties of various ionic liquid such as viscosity, conductivity, thermal stability via DSC and TGA, in order to replace conventional electrolytes with ionic liquids keeping high anodic stability and thermal stability. Among candidates, 1-allyl-3-vinyl imidazolium bis(trifluoromethanesulphonyl)imide [AVIm][TFSI] is selected to one of promising ionic liquid as new additives because it shows improved cycle life and rate properties and increased discharge capacity, thus, they propose that ionic liquid also can be applied as solvents and additives.²⁸

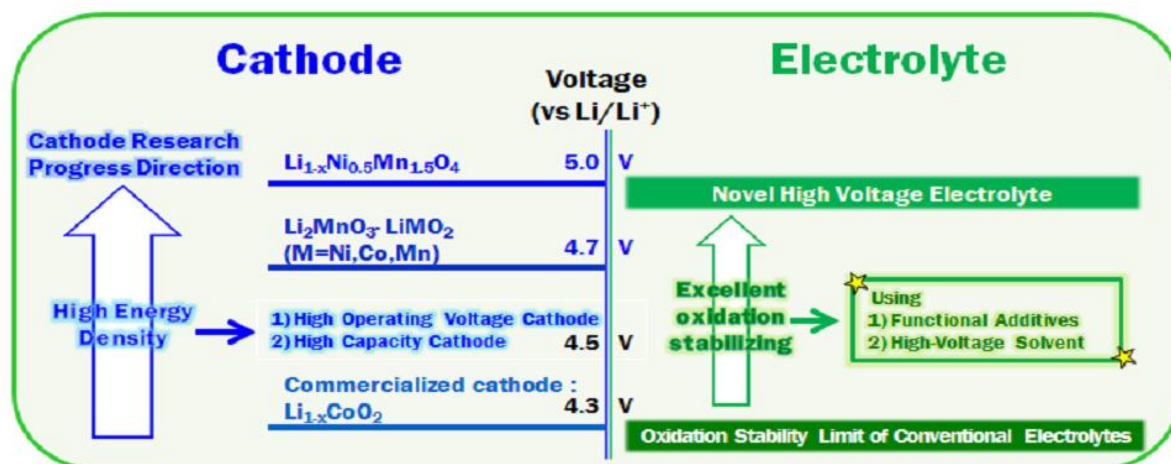


Fig. 1-8 Strategies to stable high-voltage $\text{LiNi}_{0.5}\text{Mn}_{1.5}\text{O}_4$ cathode. (1) Add additive for stable solid electrolyte interphase (SEI) layer, (2) Replace solvent for high anodic stability.

short name	structure	computed V_{ox} (V)
EMS		6.11
MEMS		5.24
EMES		5.39
F-MEMS		5.82
F-EMES		5.82

Fig. 1-9 Comparison of molecular structures and computed Oxidation Potential (V_{ox}).²⁶

1.2. Backgrounds of my research

1.2.1 Electrolyte

Electrolyte is essential component that is composed of solvent and salt in lithium ion battery to transport lithium ion that make it possible for chemical energy to convert electric energy from cathode to anode during charge/discharge process, and takes part in formation of SEI layer between electrode and electrolyte after flow of electron through external circuit.

Roles of electrolyte is bellow

- Dissociation of lithium salt

(Dissociation: a process splitting ion compounds (slats) into ions)

- Migration of solvated lithium ion between two electrodes

- Electrochemical reaction at the interphase

In terms of organic solvents, to improve electrochemical performance, there are a lot of considerations such as high ionic conductivity, low viscosity, high dielectric constant (dissociation of ion compounds), stability toward electrode (wide electrochemical window), low melting point and high boiling point (extensive operating temperature), high flash point (safety issue), miscibility between slat and solvent, wettability to separator, inert to all cell components, and so on. Generally, organic solvents consist of cyclic or linear carbonate (Fig. 1-10). Cyclic and linear carbonates entirely behave like two different kinds in terms of viscosity and dielectric constant. While cyclic carbonates indicate high dielectric constant due to partial polar structure that means it has ability to easily dissociate and high viscosity, linear carbonates show low dielectric constant and viscosity (Fig 1-11). So, they should be suitably mixed to supplement each disadvantage.

There are many kinds of lithium salts such as LiPF_6 , LiBF_4 , LiBOB , LiFOB , LiClO_4 , LiAsF_6 , LiSO_3CF_3 . Because they has different characters of conductivity or solubility, it is essential to consider what kind of lithium salt is selected. There are many requirements of lithium salt to improve electrochemical properties; thermal and electrochemical stability, good solubility, chemical stability, high conductivity, low cost, and so on. Although LiPF_6 is commercialized as lithium salt in LIBs, it has some demerits of chemical and thermal instability and generation of HF when meeting trace of water. Moreover, PF_5 generated LiPF_6 tends to initiate ring-opening polymerization or cleavage of ether linkages. Therefore, I think it is important to substitute LiPF_6 with some lithium salt in order to increase electrochemical performance.

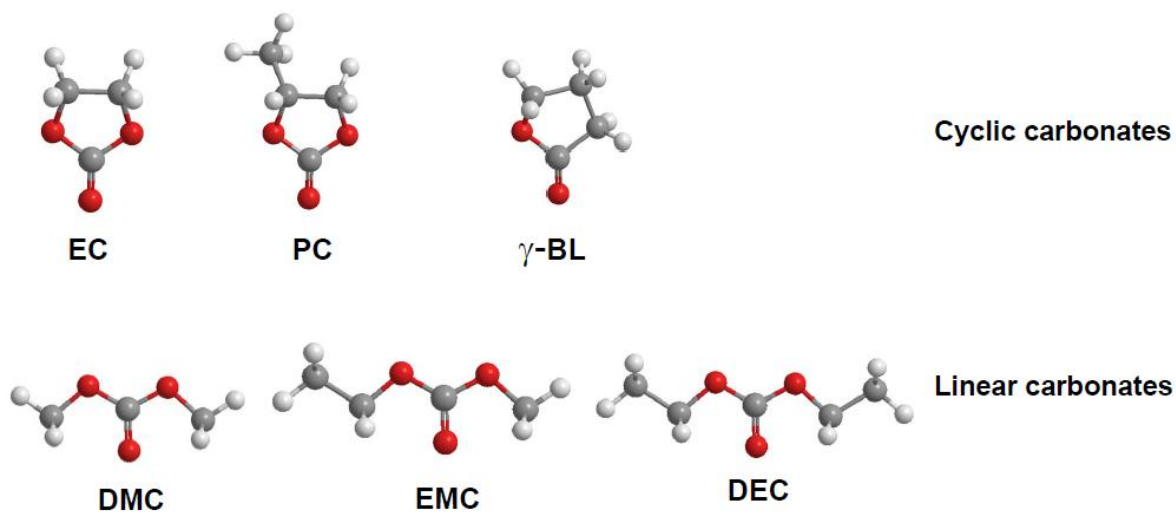


Fig. 1-10 Molecular structure of typical cyclic and linear carbonates.

Organic solvent	b.P (°C)	m.P (°C)	Dielectric constant	Viscosity (c poise)
EC (ethylene carbonate)	248	36	89.6	1.9 (40°C)
PC (propylene carbonate)	424	-49	64.9	2.5
γ -BL (g-butyrolactone)	206	-42	39.1	1.75
DMC(dimethyl carbonate)	90.3	4	3.12	0.63
DEC (diethyl carbonate)	126	-43	2.4	0.75
EMC (ethyl methyl carbonate)	107	-55	2.84	0.68

Fig. 1-11 Properties of organic solvents.

1.2.2 Solid electrolyte interphase (SEI) layer

One of the important roles is discussed in section 1.2.1; Electrochemical reaction at the interphase. Because range of oxidative or reductive decomposition of electrolyte which is currently commercialized is limited around 0.7 V ~ 4.3 V vs Li/Li⁺, electrolyte participates in electrochemical reaction at the interphase and form passivation film along with consume Li⁺ ion and electron on the surface between electrode-electrolyte due to wide operating electrochemical range of LIBs. For example, operating potential of the spinel LiNi_{0.5}Mn_{1.5}O₄ applied to cathode is over 4.7 V, thus, electrolyte decomposition inevitably occurred and form passivation film. This produced film is called as solid electrolyte interphase (SEI) layer (Fig. 1-12).

Usually, it is composed of partially insoluble inorganic material from decomposition of lithium salt and soluble reduction products of electrolyte components. The thickness of SEI layer differs from a few Å to hundreds of Å, and components comprising SEI layer can be changed depending on types of electrolyte. According to components of SEI, the cell performance will be significantly affected such as rate capability, cycle performance, self discharge, resistance, electrochemical stability, and so on. The desirable SEI layer is electronic insulator including low internal resistance, high faradaic efficiency and uniform morphology and chemical composition for homogeneous current distribution

Therefore, lots of researchers have been studying to modify SEI layer for high performance. To investigate how SEI layer can be changed, I will discuss that in section 1.3.2.

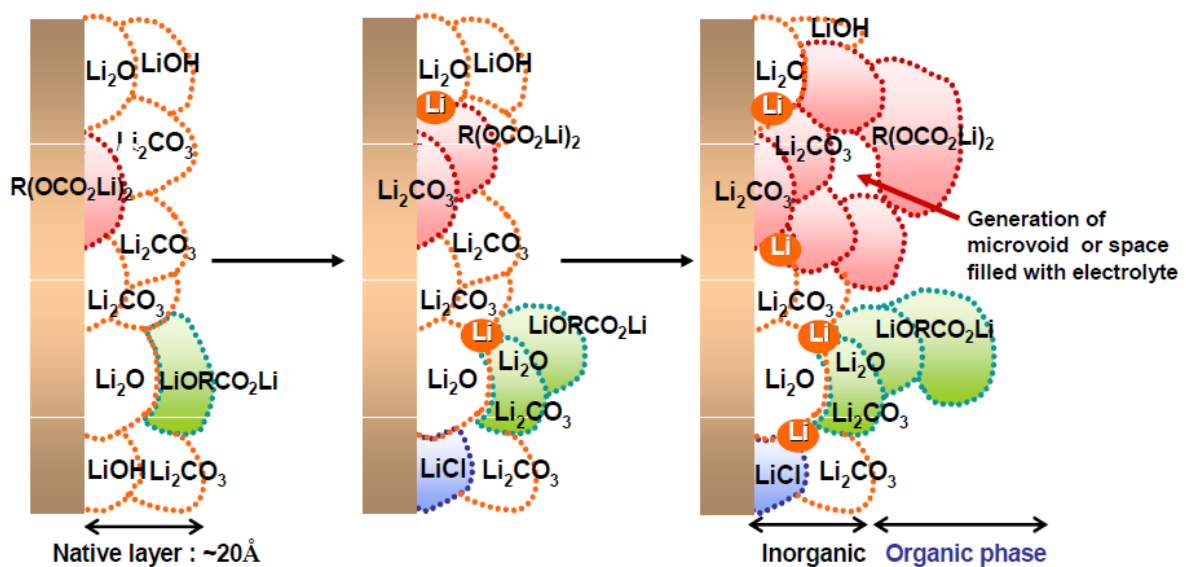


Fig. 1-12 Presentation of SEI lay and process of growth as cycle goes on.

1.3.2 Electrolyte additives

In the previous section, I mention that SEI layer is produced by electrolyte decomposition during a few cycle and we investigate how to modify components of SEI layer to improve electrochemical performance.

To modify SEI layer, small amount of additives are included in electrolyte with less than 5% either by volume or by weight amount of electrolyte. It is very effective way because a little amount of additives sufficiently affects cell performance of LIBs and there is no complicated process only by adding additive into electrolytes, and it is reasonable in term of cost.

Inserting additive is able to improved electrochemical performances such as long-term cycling, suppress gas generation and transition metal dissolution of cathode, help SEI layer to have less resistance and fast charge transfer, enhance safety thermal stability.

To design SEI layer, it is important to confirm molecular orbital of additives because molecular orbital implies tendency of oxidative or reductive decomposition comparing to components of baseline electrolyte. There are two kinds of molecular orbital. One is highest occupied molecular orbital (HOMO) and another is lowest unoccupied molecular orbital (LUMO) energy level. To change cathode surface, HOMO energy levels can be utilized to predict the oxidation tendency of additives, because some material which has higher energy level prefers to lose their electron during charge state, thus, it is easily decomposed and covered onto the cathode surface. Against to this case, the additives for negative electrodes must have lower LUMO energy because they undergo reduction reaction to develop SEI layer on the surface of anode.

Through this prediction, it is possible to narrow candidates as an additive and reduce trial and error, and the representation regarding behavior of HOMO and LUMO is indicated in Fig. 1-13.

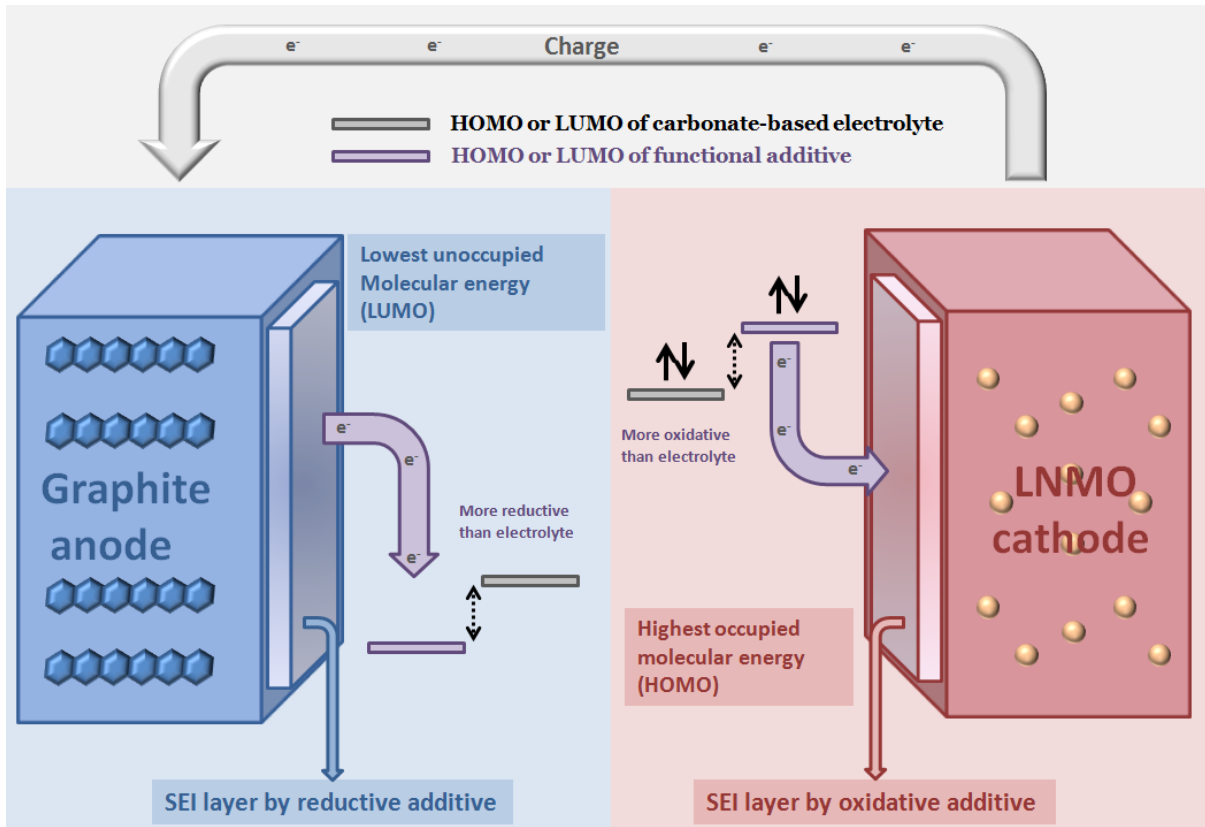


Fig. 1-13 Molecular orbital energies of additive and carbonate-based electrolyte and electron movement according to their molecular orbital energies.

CHAPTER II

The promising candidate as functional additive for $\text{LiNi}_{0.5}\text{Mn}_{1.5}\text{O}_4$ cathodes with superior electrochemical performance

2.1 Introduction

Lithium-ion batteries (LIBs) which considered as candidate to solve economic considerations and to substitute depleted nature resources have been furthered as the most energy source for energy portable devices such as cellular phones, camera, tablet PC.²⁹ Even though LIBs have been successfully commercialized, a noticeable improvement in energy density of Li-ion cells is required to satisfy higher capacity and power density (Fig. 2-1). High energy density in a battery can be obtained either by increase operating potential and capacity in terms of cathode or by decrease operating potential and increase capacity in terms of anode (Fig. 2-2). To satisfy this qualifications, $\text{LiNi}_{0.5}\text{Mn}_{1.5}\text{O}_4$, which operates in the vicinity of 4.7 V vs. Li/Li^+ and can deliver a capacity up to 147mAh g^{-1} g and thus has 680Wh Kg^{-1} , has been investigated as a promising material for LIBs of cathode with high energy densities as well as cheap cost. However, several issues including severe oxidative decomposition of carbonate-based electrolyte and LiPF_6 salt which commercialized in LIBs due to its low oxidative stability at around 4.3V, self-discharge at elevated temperature, and transition metal dissolution should be discussed prior to application.^{17,18} Also other critical problem occurred from HF which produced by reaction between the trace of water in the electrolyte and LiPF_6 . It is well known that reaction by HF to $\text{LiNi}_{0.5}\text{Mn}_{1.5}\text{O}_4$ at elevated temperatures is one of the important reasons for capacity fading, the decomposition of electrolyte, and deteriorating the electrochemical performance of cathode material.³²⁻³⁶ Resultingly, large irreversible capacity and low coulombic efficiency are observed, when $\text{LiNi}_{0.5}\text{Mn}_{1.5}\text{O}_4$ are adopted to cathode because of the problems mentioned above.^{37,38}

To alleviate the oxidative decomposition of electrolyte due to high voltage, sulfone-based solvents, ionic liquids, and dinitrile solvents have been explored, as they are appearing high anodic stabilities. Unfortunately, these solvents suffer from high intrinsic viscosities and severe reductive decomposition on carbonaceous anode materials.²¹⁻²⁵ Along with these attempts of proposed solvents having high anodic stability, some of materials are investigated as one of the effective additives and salt alternating LiPF_6 .³⁴⁻³⁹ Even though there are lots of research results by now, electrolyte additives for stabilizing the high-voltage cathode-electrolyte interphase, high-voltage electrolyte systems with superior

electrochemical stability at high-voltage cathodes should be developed. high-voltage electrolyte systems should have many fastidious requirements in Figure. 2-3.

Herein, we introduce, for the first time, one of promising multifunctional additives, tris(trimethylsilyl) phosphite (TMSP), to suppress electrolyte decomposition at high voltage, and to eliminate HF facilitating the transition metal dissolution from $\text{LiNi}_{0.5}\text{Mn}_{1.5}\text{O}_4$ cathode. Furthermore, to convince the practical impact and additional function of phosphite-type additive, we present progressive study comparing TMSP with other additives commonly retaining phosphite core. In addition, from an analysis of surface chemistry of SEI layers on the high voltage cathode, we can find similar components of SEI layers formed by various phosphite-added electrolytes via ex situ X-ray photoelectron spectroscopy (XPS), and propose its common functions which eliminate HF and alleviate decomposition of LiPF_6 by hydrolysis via nuclear magnetic resonance (NMR).

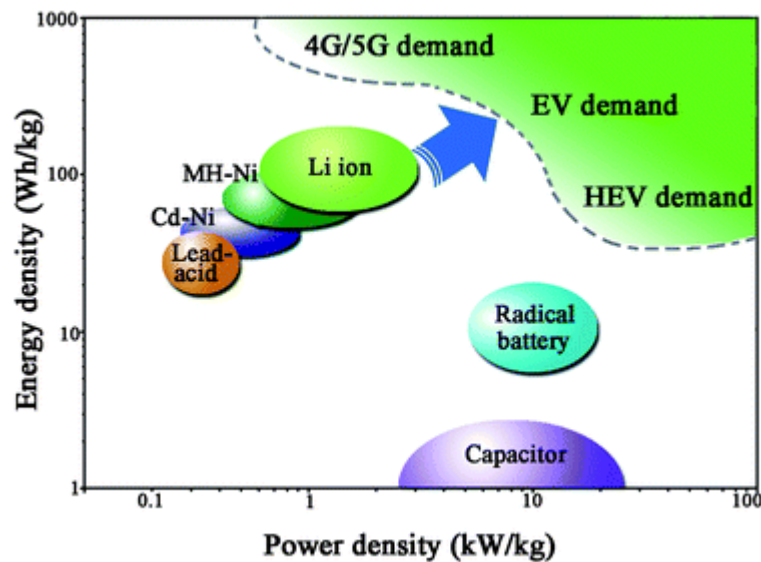


Fig. 2-1 Schematic representation of the different secondary batteries in terms of power density and energy density.⁶⁴

$$\text{Energy density} = \text{Capacity} \times \text{Working potential}$$

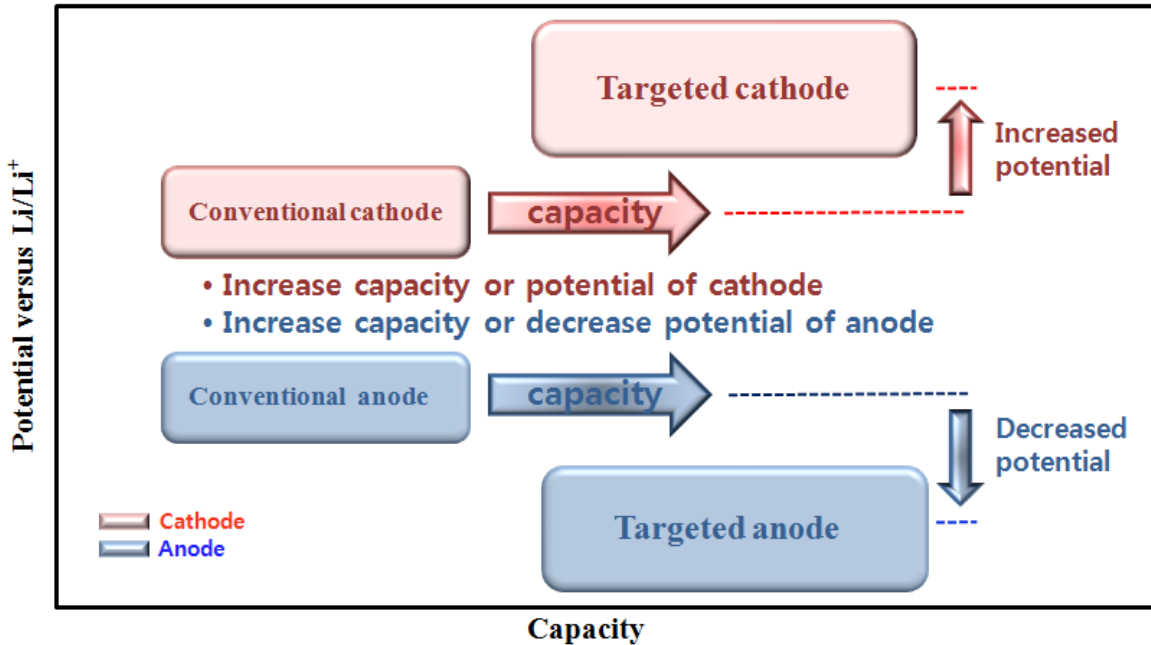
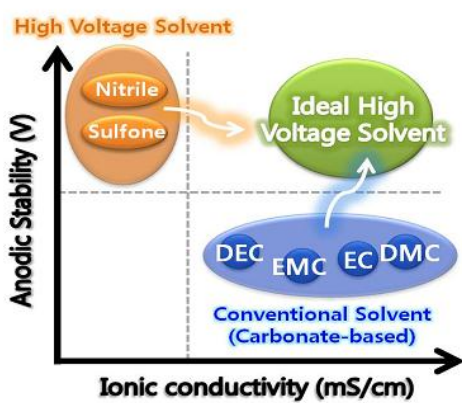


Fig. 2-2 Strategies to increase energy density of LIBs.



- Fastidious requirements of high-voltage solvent-based electrolyte**
- High oxidation stability (> 5.2 V)
 - High conductivity (> 5×10^{-3} S/cm, 25 °C)
 - Low viscosity (< 3.0 cp, 25 °C)
 - Low melting point (< -30 °C)
 - Form a stable SEI layer on the electrode

Fig. 2-3 Oxidation stability and ionic conductivity of desirable high voltage solvent-based electrolytes.

2.2 Experimental

2.2.1 Electrolyte and electrode preparation

The electrolyte with and without 0.5% triphenyl phosphite (TPP, Aldrich.), 0.5% trimethyl phosphite (TMP, Aldrich.), tris(2,2,2-trifluoroethyl) phosphite (TFEP, Aldrich.), tris(trimethylsilyl)phosphite (TMSP, Aldrich) was composed of commercially available 1.0M lithium hexafluoro phosphate (LiPF_6) dissolved in a solvent mixture of ethylene carbonate (EC), ethylmethyl carbonate (EMC), and dimethyl carbonate (DMC) with a 3:4:3 volume ratio. TPP, TMP, TFEP, TMSP were used as received and introduced as an additive to form the surface film on $\text{LiNi}_{0.5}\text{Mn}_{1.5}\text{O}_4$ cathodes. A slurry was prepared by mixing 90 wt.% of $\text{LiNi}_{0.5}\text{Mn}_{1.5}\text{O}_4$ particles (GS energy and materials Co. Ltd.), 5 wt.% of carbon black as a conducting material and 5 wt.% of a polyvinylidene fluoride (PVdF) binder dissolved in anhydrous N-methyl-2-pyrrolidinone (NMP). The resulting slurry was cast on aluminum foil and then dried at 110°C for 30 min in a convection oven. The electrode was next pressed and its thickness was around $34\ \mu\text{m}$. The specific capacity of the cathode and the active material loading were $0.45\ \text{mAh cm}^{-2}$ and $3.97\ \text{mg cm}^{-2}$, respectively.

2.2.2 Electrochemical Measurements

A coin-type half cell (2032) with a cathode $\text{LiNi}_{0.5}\text{Mn}_{1.5}\text{O}_4$ cathode and a Li metal electrode was assembled in an argon-filled glove box with less than 1 ppm of both oxygen and moisture. Thickness and porosity of a microporous polyethylene film (SK innovation Co.Ltd.) used as a separator were $20\ \mu\text{m}$ and 38%, respectively.

Galvanostatic charge and discharge process (WonATech WBCS 3000 battery measurement system) was performed at first cycle in the potential window from 3.5 V to 5.0 V versus Li/Li^+ with $\text{LiNi}_{0.5}\text{Mn}_{1.5}\text{O}_4/\text{Li}$ 2032 coin-type half cell. Charge and discharge rate was 0.5C rate in the potential range between 3.5 V and 5.0 V during cycling after 0.2C rate in precycling process.

To investigate rate capability of $\text{LiNi}_{0.5}\text{Mn}_{1.5}\text{O}_4$ cathodes, the cells were charged and discharge using various C rate from 0.5 C to 5 C during discharge and same charge rate at 0.5C at 30°C .

2.2.3 Characterization

Cell impedances of the half cells after precycling were measured by AC impedance analysis with an IVIUM frequency response analyzer over a frequency range of 0.01Hz to 1MHz, perturbation amplitude 5mV.

After precycling, the cells were opened in a glove box to retrieve their electrodes. The electrodes were then rinsed in dimethyl carbonate (DMC) to remove the residual LiPF₆-based electrolyte. These electrodes were used for ex-situ X-ray photoelectron spectroscopy (XPS, Thermo Scientific K-Alpha system) and ex-situ field emission scanning electron microscope (FE-SEM; JEOL JSM-6700F) measurement with energy-dispersive X-ray spectroscopy (EDS) in the electrolyte with and without variable additives. Ex-situ X-ray photoelectron spectroscopy measurements for dried cathodes were performed using Al K α ($h\nu = 1486.6$ eV) radiation under ultrahigh vacuum. XPS spectra were taken using a 0.10 eV step and 50 eV pass energy. All XPS spectra were calibrated by the hydrocarbon peak at the binding energy of 284.8eV. All the samples were prepared in a glove box and sealed with an aluminum pouch film under a vacuum before use.

X-Ray diffraction (XRD) data was collected on Bruker AXS D2 diffractometer using Cu K α radiation and operating from $2\theta = 10^\circ - 80^\circ$. The patterns were analyzed by using software from Bruker AXS.

¹⁹F and ³¹P NMR spectra were recorded on a Agilent (VNMRS 600) spectrometer, and THF-d₈ was used as a solvent. 5 vol% water was added to baseline and phosphite-added electrolytes and the outputs were stored in NMR tube during 22 h at room temperature and the resulting solutions finally were analyzed.

2.3. Results and discussion

2.3.1 Improved electrochemical performance by using TMSP additive

The oxidation tendency of organic molecules can be predicted by calculating the highest occupied molecular orbital (HOMO) energy level. Fig. 1 shows the HOMO energy as well as the lowest unoccupied molecular orbital (LUMO) energy of ethylene carbonate (EC) as a conventional carbonate solvent and reducible additives such as vinylene carbonate (VC) and fluoroethylene carbonate (FEC), which have been identified as the most efficient anode SEI formers.²⁹ Appropriate additives making a protective layer on the high voltage $\text{LiNi}_{0.5}\text{Mn}_{1.5}\text{O}_4$ cathode without the reductive decomposition should have analogous LUMO energy and higher HOMO energy relative to carbonate solvents. In this point of view, tris(trimethylsilyl) phosphite (TMSP) including an inorganic phosphorous (III) core surrounded by three $-\text{O}-\text{Si}(\text{CH}_3)_3$ moieties is predicted to oxidize on the cathode without appreciable reduction on the anode (Fig. 2-4). The HOMO of TMSP is situated at the P–O groups displaying the donor character. It is expected that these donor groups will undergo the electrochemical oxidation at high potential and contribute to the formation of the SEI on the cathode. Moreover, hydro fluoric acid (HF), which is inevitably generated from the decomposition of PF_5 in the presence of water traces, may readily attack the Si–C groups with a low bond energy of 318 kJ mol^{-1} and thereby HF promoting Mn/Ni dissolution from $\text{LiNi}_{0.5}\text{Mn}_{1.5}\text{O}_4$ cathodes may be eliminated from the electrolyte.

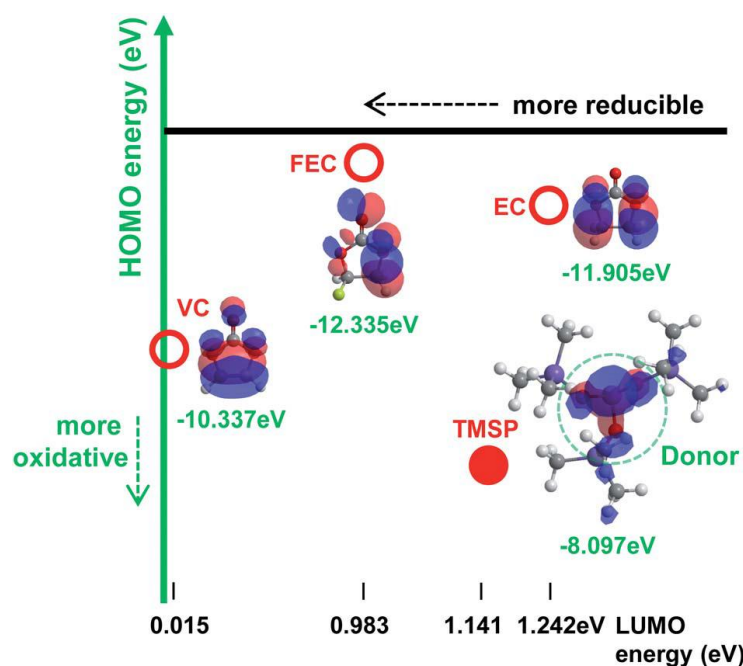


Fig. 2-4 The calculated highest occupied molecular orbital (HOMO) and lowest unoccupied

molecular orbital (LUMO) energy levels of TMSP, VC, FEC additives and an EC solvent. The HOMO is situated at the electron-rich moieties showing the donor character.

A comparison of the cycling stabilities of $\text{LiNi}_{0.5}\text{Mn}_{1.5}\text{O}_4$ cathodes with and without the TMSP additive at a current density of 60 mA g^{-1} is presented in Fig. 2-5. Surprisingly, an excellent cycling stability of the $\text{LiNi}_{0.5}\text{Mn}_{1.5}\text{O}_4$ cathode at 60°C and a current density of 60 mA g^{-1} was achieved in the TMSP-added electrolyte, delivering a capacity of 110 mA g^{-1} without a noticeable capacity loss over 100 cycles. The discharge capacity retention was drastically improved from 66.5% (baseline electrolyte) to 82.1% (TMSP-containing electrolyte) after 160 cycles at 60°C . The cell cycled in the TMSP-added electrolyte displayed a high capacity retention of ca. 90% in the 100th cycle. This lower capacity fade with cycling can be explained by the formation of a TMSP-derived SEI layer on the $\text{LiNi}_{0.5}\text{Mn}_{1.5}\text{O}_4$ cathode.

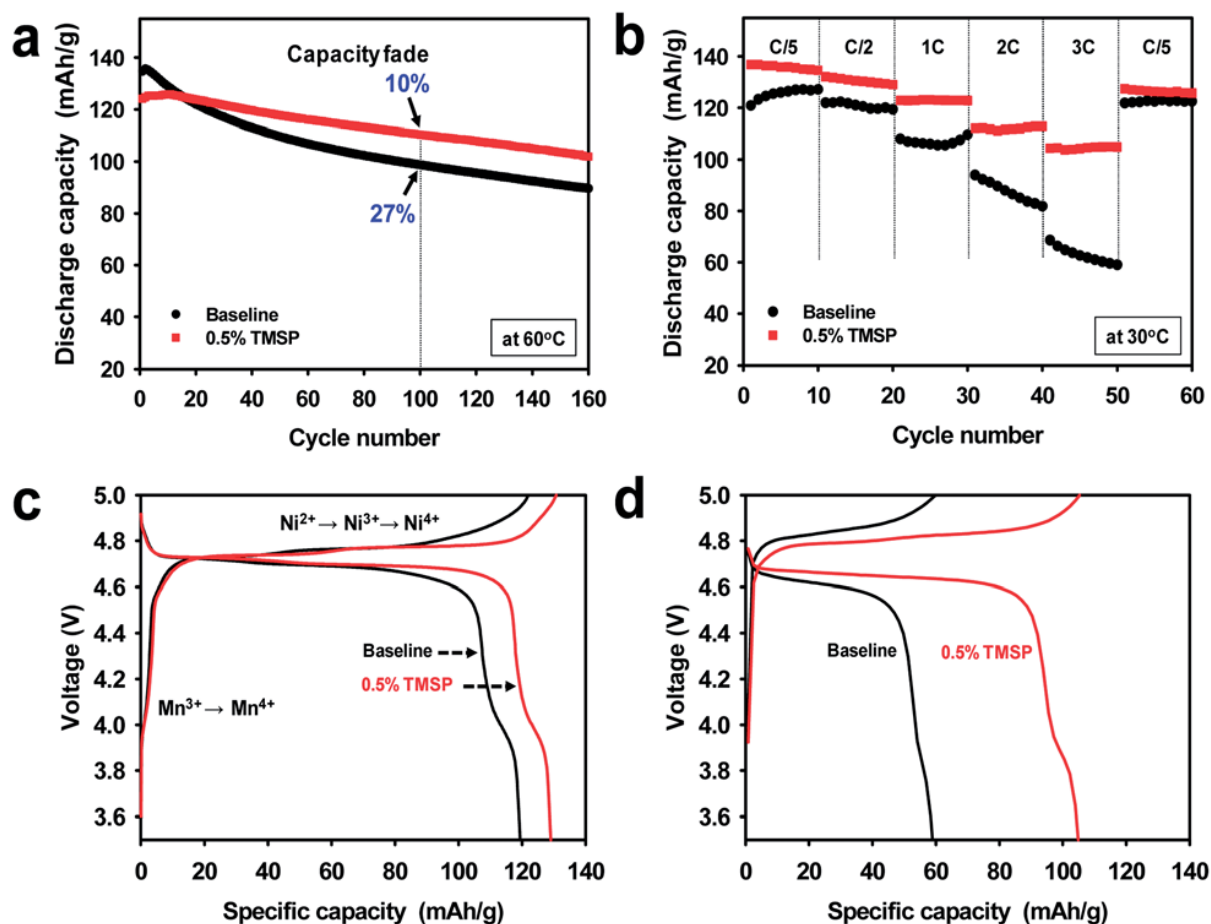


Fig. 2-5 Electrochemical performance of $\text{LiNi}_{0.5}\text{Mn}_{1.5}\text{O}_4$ cathodes: (a) cycling stability when cycled between 3.5 and 5.0 V at a rate of C/2, (b) rate capability at different C rates, (c) charge and discharge curves at a rate of C/2, and (d) charge and discharge curves at a rate of 3 C.

This SEI layer inhibits direct contact of the electrolyte components with the high-voltage cathode and, thus, effectively diminishes the continuous oxidative decomposition of the electrolyte solution upon prolonged cycling at 60 °C. The discharge capacity fading of cells with the conventional (baseline) electrolyte was much stronger than that of cells using the TMSP-added electrolyte in subsequent cycles (Fig. 2-5a). This is consistent with the result that a fully charged $\text{Li}_x\text{Ni}_{0.5}\text{Mn}_{1.5}\text{O}_4$ cathode stored in the TMSP-added electrolyte at 60 °C shows better storage performance (Fig. 2-6). The $\text{LiNi}_{0.5}\text{Mn}_{1.5}\text{O}_4$ cathodes cycled in FEC- and VC-containing electrolytes exhibited considerably reduced discharge capacities and inferior cycling stabilities compared to the cells with TMSP, which showed a noticeable improvement in cycling stability (Fig. 2-7). The cathodes with VC- and FEC-added electrolytes delivered very low discharge capacities of 72 and 42 mAh g^{-1} in the 160th cycle, respectively. This implies that the FEC and VC additives could not preserve the electrochemical properties of the high voltage cathodes because of the vulnerabilities of the FEC- and VC-derived SEI layers under high voltage conditions.

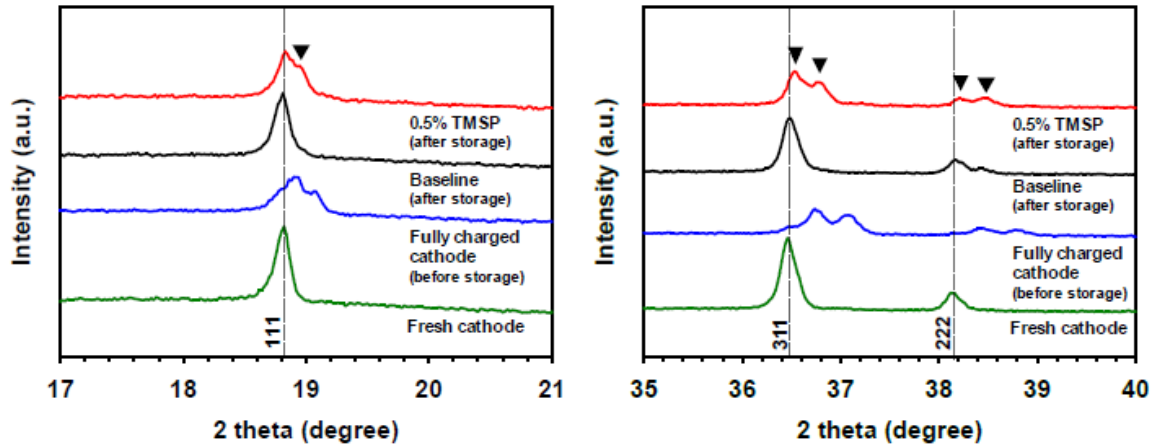


Fig. 2-6 XRD patterns of fully charged $\text{Li}_x\text{Ni}_{0.5}\text{Mn}_{1.5}\text{O}_4$ cathode before and after stored at 60°C for 1 day. The XRD pattern of fresh $\text{LiNi}_{0.5}\text{Mn}_{1.5}\text{O}_4$ cathode is displayed for comparison. The XRD data reveals that a fully charged cathode stored in the TMSP-added electrolyte at 60°C experiences less delithiation (self-discharge).

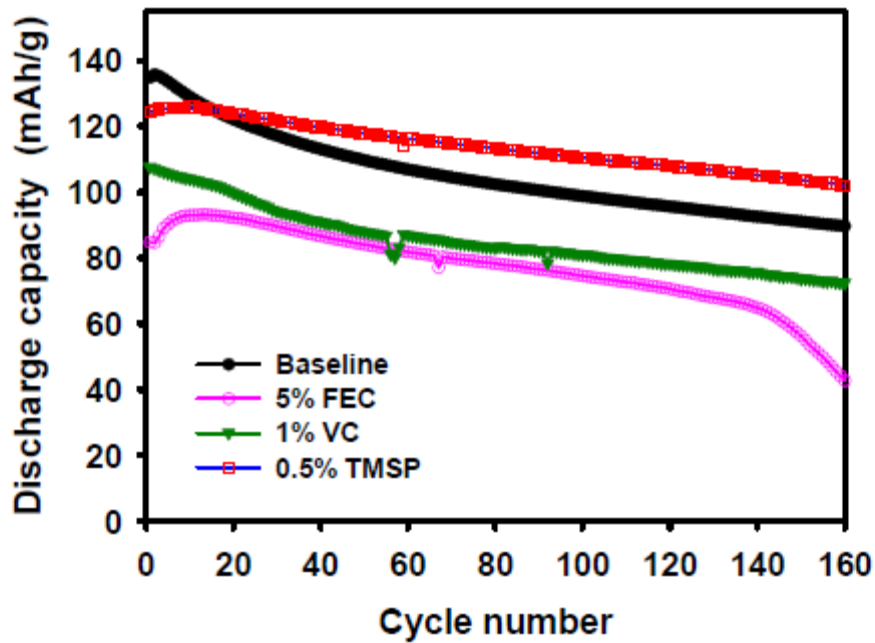


Fig. 2-7 Comparison of cycling stability of $\text{LiNi}_{0.5}\text{Mn}_{1.5}\text{O}_4$ cathodes with various electrolytes at 60°C

at a current density of 60 mA g⁻¹.

To further conform the positive impact of the TMSP additive on the electrochemical properties of the cathode, galvanostatic cycling of Li/ LiNi_{0.5}Mn_{1.5}O₄ cells was performed at a current density of 60 mA g⁻¹ and 30 °C (Fig. 2-8). Clearly, the discharge capacity of the cell with the TMSP-added electrolyte during cycling was comparable with that of the cathode with the baseline electrolyte. A major challenge for the implementation of LiNi_{0.5}Mn_{1.5}O₄ cathodes is undesirable electrolyte decomposition at high voltage, as evidenced by the previously reported low coulombic efficiency of ca. 97% for Li/ LiNi_{0.5}Mn_{1.5}O₄ cells at room temperature.⁴⁰ Interestingly, the Li/ LiNi_{0.5}Mn_{1.5}O₄ half cells cycled in the TMSP-added electrolyte displayed a significant coulombic efficiency improvement of ca. 99% during cycling at 30 °C (Fig. 2-8). This result suggested that the TMSP-derived SEI was sufficiently robust to suppress continuous electrolyte decomposition at 30 °C and effectively reduced irreversible capacity during cycling.

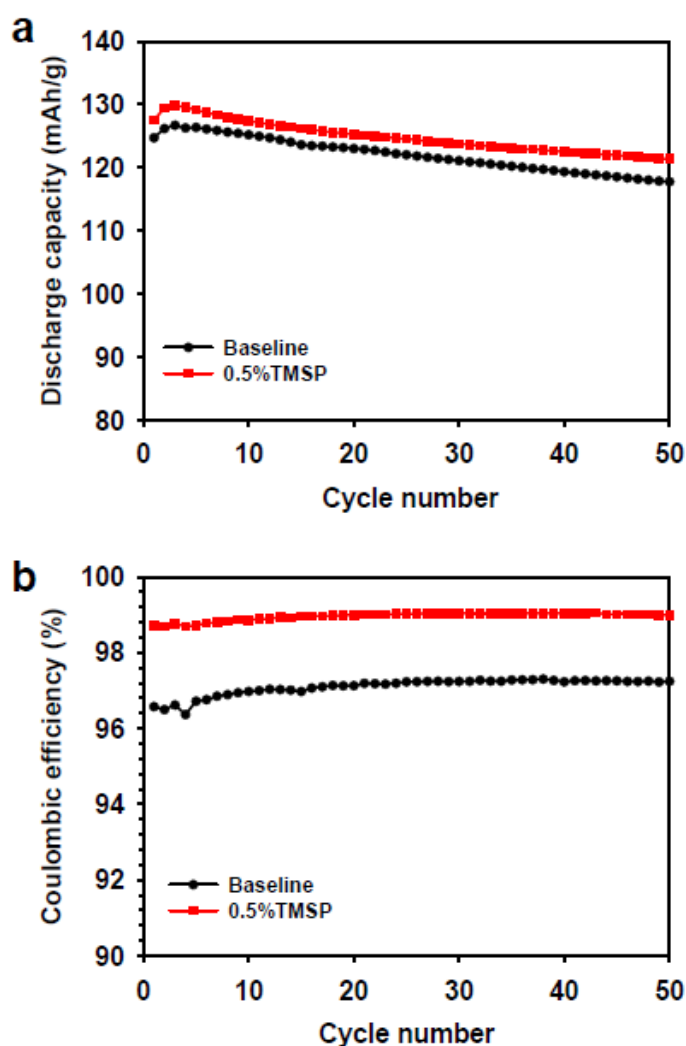


Fig. 2-8 (a) Discharge capacity, (b) Coulombic efficiency of the $\text{LiNi}_{0.5}\text{Mn}_{1.5}\text{O}_4$ cathodes in baseline and TMSP-added electrolytes at 30 °C at a current density of 60 mA g⁻¹.

To investigate the suitability of the TMSP-derived SEI for facilitating charge transfer at the cathode surface, the cycling stability of the $\text{LiNi}_{0.5}\text{Mn}_{1.5}\text{O}_4$ cathode was investigated at high current densities (Fig. 2-5b). The TMSP-added electrolyte clearly exhibited a much superior rate capability than the baseline electrolyte. The $\text{LiNi}_{0.5}\text{Mn}_{1.5}\text{O}_4$ cathode with the TMSP additive delivered a superior discharge capacity (105 mAh g⁻¹) at a very high current density (360 mA g⁻¹, corresponding to 3 C) at 30 °C. However, the cell cycled in the baseline electrolyte showed rapid capacity fading as a function of the applied current density, and delivered a very low discharge capacity of only 60mAh g⁻¹ at 3 C.

The $\text{LiNi}_{0.5}\text{Mn}_{1.5}\text{O}_4$ cathode cycled in the TMSP-added electrolyte exhibited a lower charge plateau and a higher discharge plateau compared to the cathode with the baseline electrolyte, indicating faster kinetics (Fig. 2-5c and d). A plateau at 4.0 V attributed to the $\text{Mn}^{3+}/\text{Mn}^{4+}$ redox couple was clearly observed in the TMSP-added electrolyte, even at a high C rate of 3 C. This finding suggested that the TMSP-derived SEI allowed fast charge transfer at high C rates, while the SEI formed by the baseline electrolyte impeded the diffusion of Li ions. Further evidence is given via comparison of the resistance of the cathode after precycling (Fig. 2-9). The interfacial resistance including R_f and R_{ct} components was smaller for the $\text{LiNi}_{0.5}\text{Mn}_{1.5}\text{O}_4$ cathode precycled in the TMSP-added electrolyte. The discharge capacities of 122 mAh g⁻¹ in the baseline electrolyte and 126 mAh g⁻¹ in the TMSP-added electrolyte were recovered at a rate of C/5 (Fig. 2-5b). Considering the high potential of 5.0 V at which Li ions are extracted from the $\text{LiNi}_{0.5}\text{Mn}_{1.5}\text{O}_4$ cathode, electrolyte components will be electrochemically oxidized and the SEI may be generated on the cathode surface.

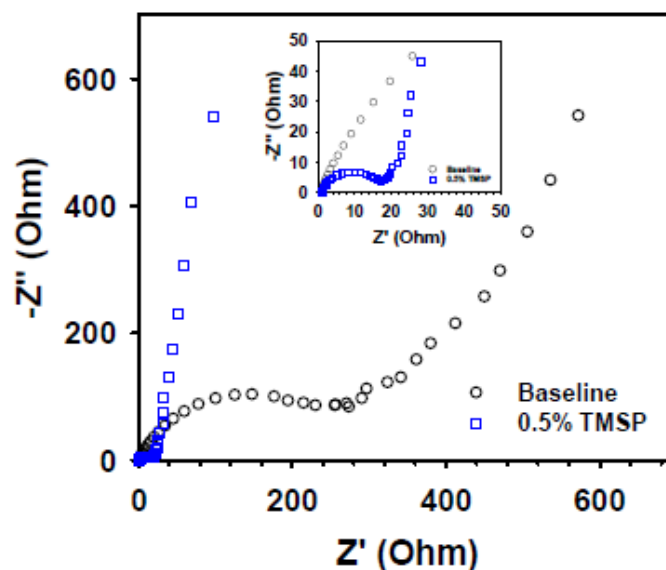


Fig. 2-9 EIS spectra for $\text{LiNi}_{0.5}\text{Mn}_{1.5}\text{O}_4$ cathodes precycled in baseline or 0.5% TMSP-added electrolyte.

The effects of TMSP on the surface chemistry of the $\text{LiNi}_{0.5}\text{Mn}_{1.5}\text{O}_4$ cathode were confirmed by a comparison of the XPS spectra obtained from cathodes cycled in the baseline and TMSP-added electrolytes after precycling at 30 °C and 5 cycles at 60 °C. Fig. 2-10 shows the F 1s and P 2p spectra of the SEIs formed on $\text{LiNi}_{0.5}\text{Mn}_{1.5}\text{O}_4$ cathodes cycled in the baseline and the TMSP-added electrolytes at 30 and 60 °C. The F 1s core level peaks assigned to the P–F moiety and LiF were clearly shown on the cathode surface, and the LiF peak intensity increased remarkably after 5 cycles at 60 °C in the baseline electrolyte, compared to that after the precycle at 30 °C. The labile P–F bonds of the LiPF_6 salt are highly susceptible to hydrolysis even if trace amounts of moisture are present in the electrolyte solution: i.e., $\text{LiPF}_6 (\text{sol.}) + \text{H}_2\text{O} / \text{POF}_3 (\text{sol.}) + \text{LiF} (\text{s}) + 2\text{HF} (\text{sol.})$, and $\text{PF}_5 (\text{sol.}) + \text{H}_2\text{O} / \text{POF}_3 (\text{sol.}) + 2\text{HF} (\text{sol.})$.⁵⁶⁻⁵⁸ The resulting HF severely consumes Li ions to form LiF as a cathode SEI component in the baseline electrolyte during cycling and causes the loss of active Li^+ ions. Moreover, the dissolution of Mn^{2+} ions from $\text{LiNi}_{0.5}\text{Mn}_{1.5}\text{O}_4$ can take place in the presence of HF and additional LiF may be formed on the cathode, as displayed in fig. 2-10. However, the LiF peak in the SEI on the cathode cycled in the TMSP-added electrolyte had a much weaker intensity than that of the SEI on the cathode cycled in the baseline electrolyte.

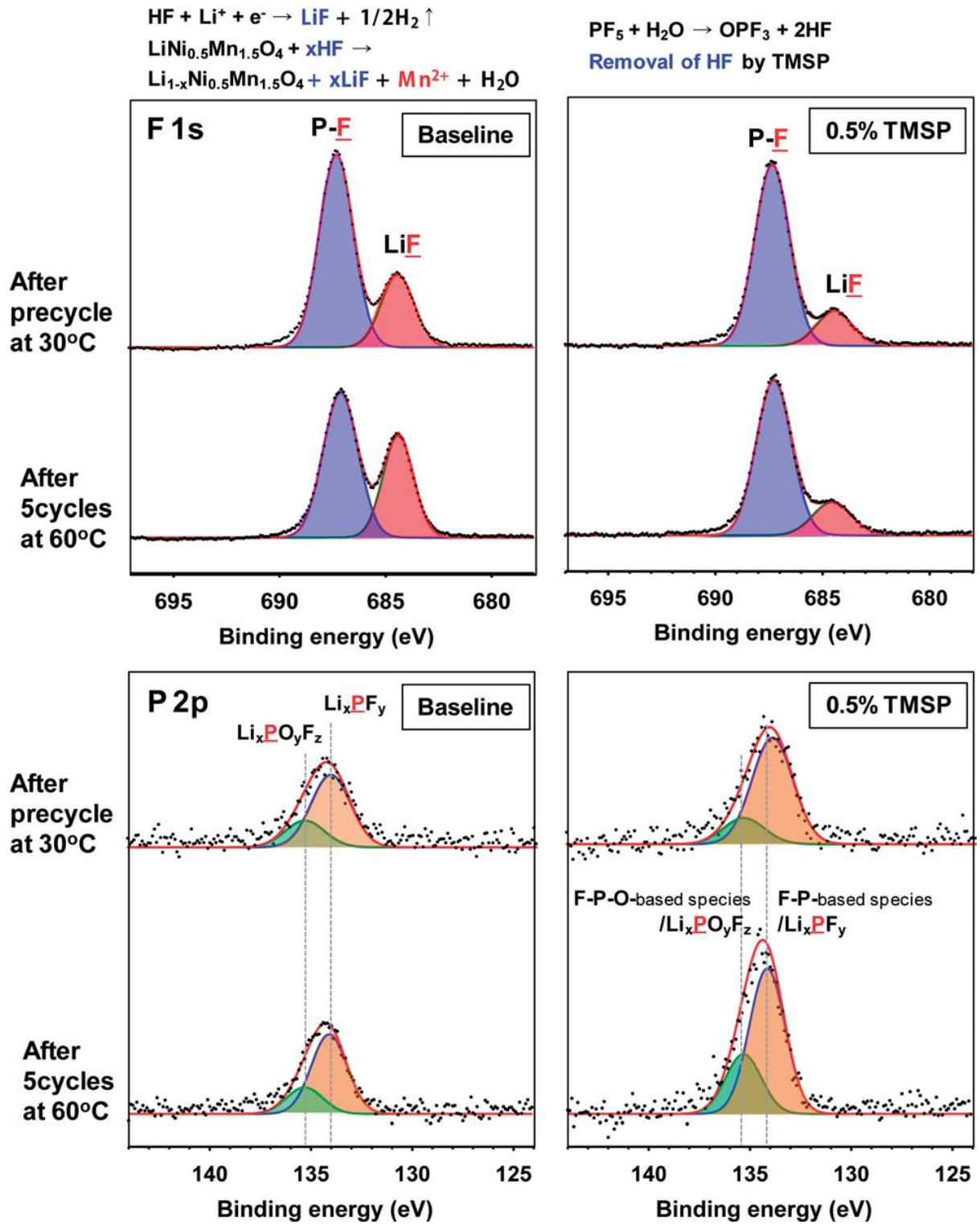


Fig. 2-10 F 1s and P 2p XPS spectra of the $\text{LiNi}_{0.5}\text{Mn}_{1.5}\text{O}_4$ cathodes after precycling at 30 °C and 5 cycles at 60 °C.

HF produced from the LiPF_6 -based electrolyte solution may be eliminated by electrochemically oxidized TMSP and by directly reacting with TMSP, as depicted in Fig. 2-11. This HF removal is thought to suppress LiF formation on the cathode. This mechanism of action for HF removal is expected to suppress the dissolution of metal ions (Mn and Ni) from the cathode. The possible mechanisms for the HF removal by the TMSP additive are displayed in Fig. 2-11.

If TMSP is not entirely consumed during SEI formation on the cathode, it can react with HF in the electrolyte solution and lead to the formation of products with $-\text{P}-\text{OH}$ or $-\text{P}-\text{O}-\text{Si}(\text{CH}_3)_{3-x}\text{F}_x$ groups (Fig. 2-11). Additionally, TMSP can produce $\text{F}-\text{Si}(\text{CH}_3)_3$ or $-\text{Si}(\text{CH}_3)_{3-x}\text{F}_x$ -containing compounds via the direct reaction with HF. The products derived from $\text{F}-\text{Si}(\text{CH}_3)_3$ or $\text{Si}(\text{CH}_3)_{3-x}\text{F}_x$ were not clearly detectable in the Si 2p XPS spectra of the SEI on the cathode (Fig. 2-12).

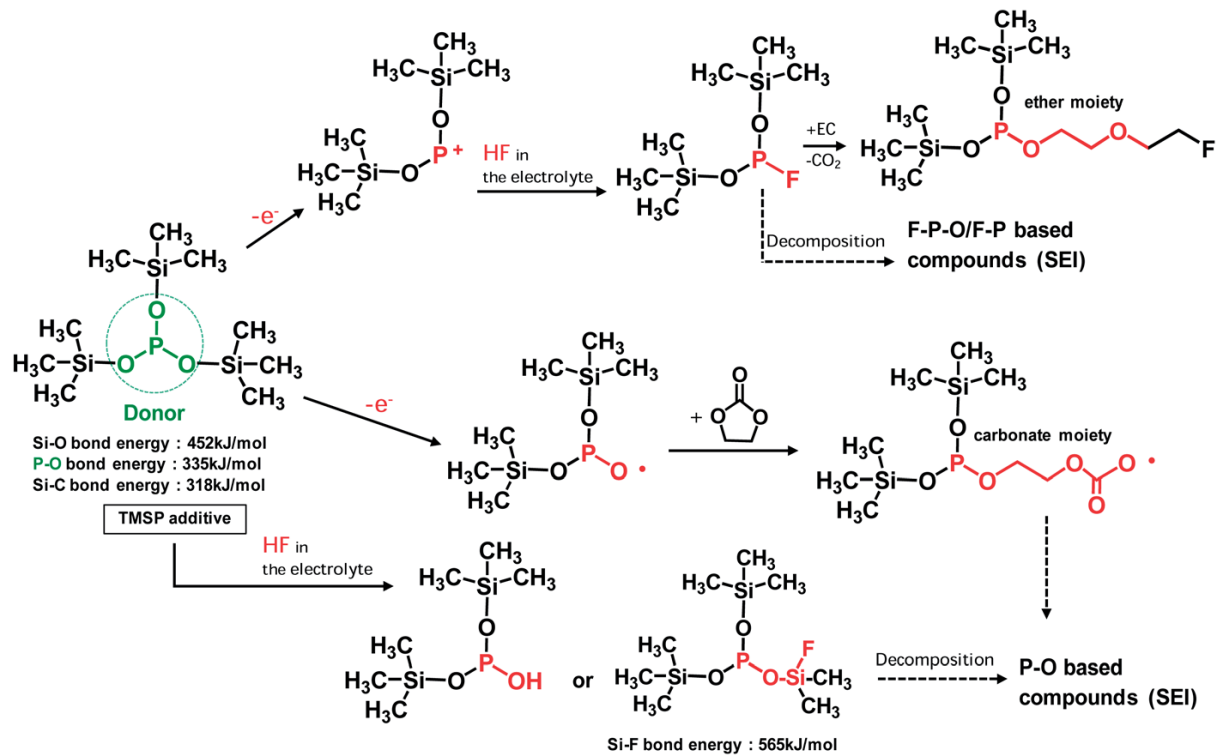


Fig. 2-11 Schematic representation of possible mechanisms for electrochemical oxidative decomposition of TMSP and unique function of TMSP scavenging HF from the electrolyte. The products produced by TMSP decomposition will contribute to the formation of the SEI on the $\text{LiNi}_{0.5}\text{Mn}_{1.5}\text{O}_4$ cathode.

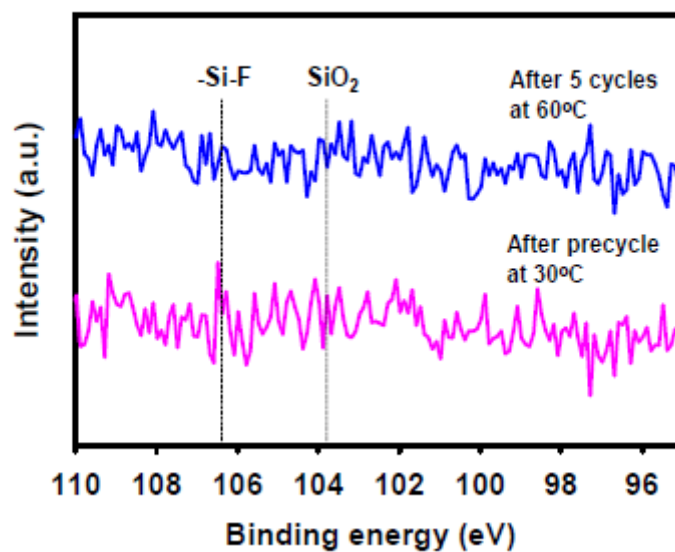


Fig. 2-12 XPS spectra of the $\text{LiNi}_{0.5}\text{Mn}_{1.5}\text{O}_4$ cathodes cycled in TMSP-added electrolyte.

To clarify the significant role of TMSP on HF removal from the electrolyte, 5 vol% water was added to the baseline and TMSP-added electrolyte solutions and the resulting solutions were stored for 22 h at room temperature. The ^{19}F NMR spectrum of the baseline electrolyte with 5 vol% water showed three different doublets consistent with a single phosphorous coupled to each fluorine (Fig. 2-13). The pronounced doublet peaks at -72 and -72.7 ppm corresponded to the PF_6^- anion. The peaks near -75 and -83 ppm could be assigned to PO_3F^{2-} and PO_2F_2^- , respectively; these were produced by the hydrolysis of LiPF_6 in the presence of water.^{52,53} Noticeable features of the TMSP-added electrolyte with 5 vol% water were the disappearance of the PO_3F^{2-} resonance near -75 ppm and prevention of LiF formation on the cathode surface by TMSP through HF produced by the hydrolysis of LiPF_6 . Indeed, the characteristic resonance of HF at -153 ppm apparently disappeared in the electrolyte with TMSP (see the ^{19}F NMR spectrum of Fig. 2-13). This result was persuasive evidence of TMSP effectively eliminating HF from the electrolyte solution, as displayed in Fig. 2-10. It should be noted that a considerable degree of Mn dissolution from the LiMn_2O_4 cathode into the electrolyte takes place in the presence of HF that is formed by the hydrolysis of LiPF_6 salts, and thereby, fast capacity fading of the cathode cannot be restrained.³⁰⁻³⁴ Similarly, Mn and Ni dissolution from the $\text{LiNi}_{0.5}\text{Mn}_{1.5}\text{O}_4$ cathode can be driven by HF attack in the electrolyte.³⁴ Surprisingly, the amount of Mn and Ni dissolution from the non-cycled $\text{LiNi}_{0.5}\text{Mn}_{1.5}\text{O}_4$ cathode stored in the TMSP containing electrolyte was negligible compared to the cathode in contact with the baseline electrolyte at 60 °C (Fig. 2-18d). This revealed that the removal of HF by the TMSP additive was very effectual in alleviating Mn and Ni dissolution from the $\text{LiNi}_{0.5}\text{Mn}_{1.5}\text{O}_4$ cathode. The P 2p spectra in Fig. 2-10 clearly showed peaks for Li_xPF_y (F-P) (at 134 eV) and $\text{Li}_x\text{PF}_y\text{O}_z$ (F-P-O) (at 135.5 eV) in the SEI on the cathodes cycled in the baseline and TMSP-added electrolytes. The intensities of these peaks discernibly increased in the TMSP-added electrolyte. This was likely because F-P-O and F-P intermediates were generated by the decomposition of TMSP upon cycling at 60 °C (see possible reactions in Fig. 2-11).

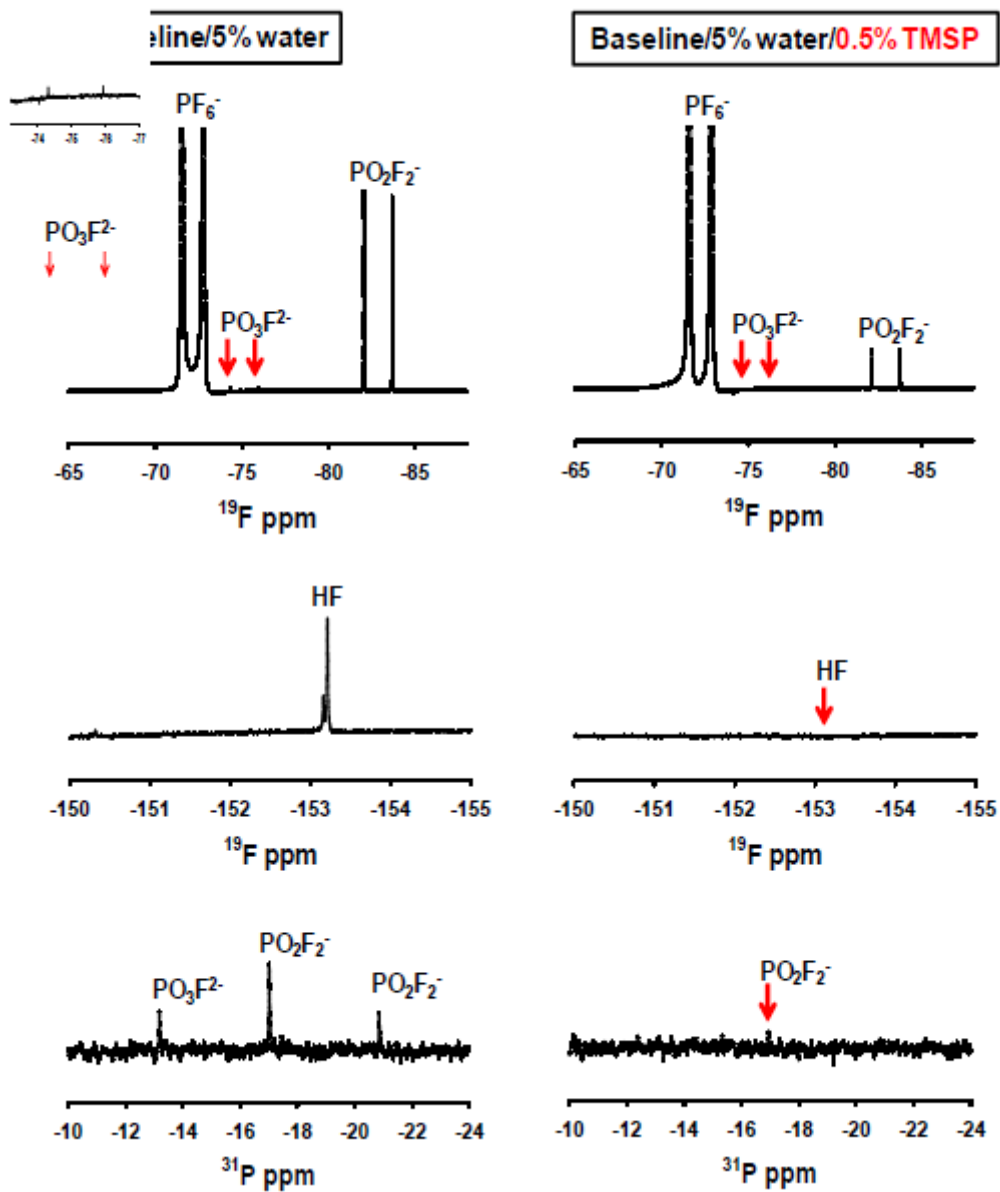


Fig. 2-13 ^{19}F and ^{31}P NMR spectra of the electrolyte with and without 0.5wt% TMSP after hydrolysis tests at room temperature. HF was completely removed from the electrolyte in presence of TMSP.

Comparison of the O 1s XPS spectra for the SEI on similarly cycled cathodes revealed that the relative fractions of carboxylate/carbonates (C=O) and ethers (C–O–C) in the TMSP-added electrolyte increased compared to the baseline electrolyte (Fig. 2-14). Ethers can be formed by the reaction between –P–F species and organic solvents such as EC, and carbonate/carboxylates can be generated by the reaction between the oxy radical (–P–O•) and EC (Fig. 2-11). From the XPS results, we confirmed that TMSP modified the surface chemistry of the SEI; the resulting SEI prevented further electrolyte decomposition during cycling and preserved the electrochemical performance of the $\text{LiNi}_{0.5}\text{Mn}_{1.5}\text{O}_4$ cathode.

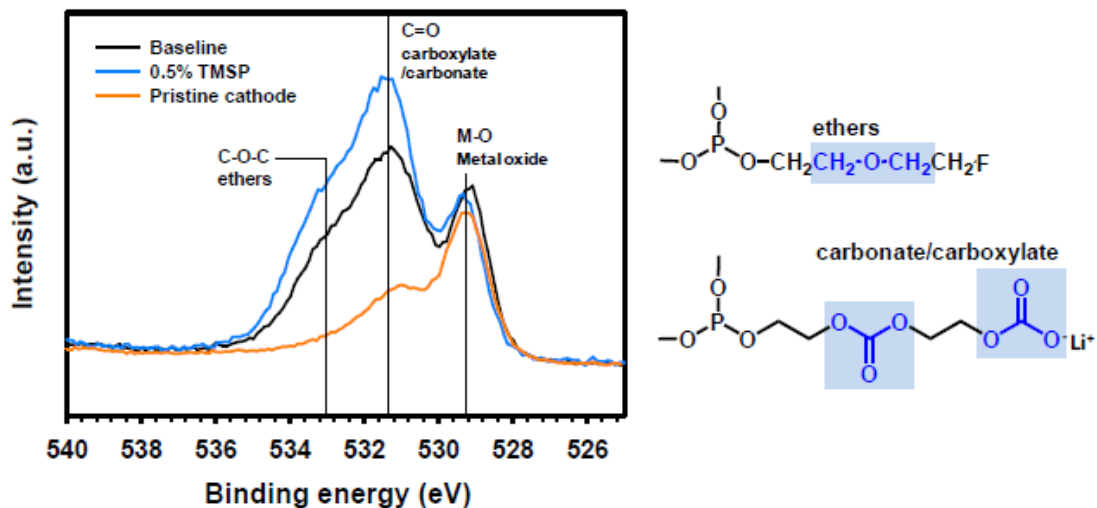


Fig. 2-14 O 1s XPS spectra of the $\text{LiNi}_{0.5}\text{Mn}_{1.5}\text{O}_4$ cathodes before and after 5 cycles in the baseline and TMSP-added electrolytes at 60 °C.

The discharge capacity retention of full cells constructed with the graphite anode, the $\text{LiNi}_{0.5}\text{Mn}_{1.5}\text{O}_4$ cathode, and the electrolyte with or without 0.5% TMSP at 30 °C is shown in Fig. 2-15a. The capacity retention at the 100th cycle is much higher for the cell containing TMSP (81%) than for the cell without TMSP (73%). Interestingly, the graphite/ $\text{LiNi}_{0.5}\text{Mn}_{1.5}\text{O}_4$ full cell cycled in the TMSP-added electrolyte exhibited a discernible improvement in coulombic efficiency (over 99.6%) upon cycling at 30 °C (Fig. 2-15b). This result was in good agreement with Fig.2-8. Galvanostatic charge–discharge curves of a full cell with TMSP clearly shows much higher discharge capacity for 1st, 30th, 50th and 80th cycles compared to the baseline electrolyte (Fig. 2-15c and d). Initial discharge and charge curves of the graphite anodes with or without 0.5% TMSP are shown in Fig. 2-16. The ICE of the graphite anode precycled in a 0.5% TMSP-added electrolyte slightly decreased from 95.3 to 95.1%. This is probably because HF removal by TMSP modified the SEI on the graphite anode. In addition, the discharge capacity retention of graphite/ $\text{LiNi}_{0.5}\text{Mn}_{1.5}\text{O}_4$ full cells with the TMSP-added electrolyte was significantly improved from 48.2 to 81.0% after 100 cycles at 45 °C (Fig. 2-17). It is thus strongly believed that TMSP predominantly modifies the cathode surface and the resulting TMSP-derived SEI on the cathode is sufficiently robust to suppress severe electrolyte decomposition under high voltage conditions.

The significant capacity fading of the graphite/ $\text{LiNi}_{0.5}\text{Mn}_{1.5}\text{O}_4$ full cell due to Mn and Ni dissolution from the cathode was similarly expected to be suppressed in the presence of TMSP eliminating HF from the electrolyte. It should be noted that a small amount of Mn and Ni ions in the electrolyte causes a significant fading of the capacity of a graphite anode because the Mn and Ni deposits are formed by consuming the electrons for intercalation of Li^+ ions into the graphite and the metallic Mn and Ni can lead to the formation of thick SEI layers.

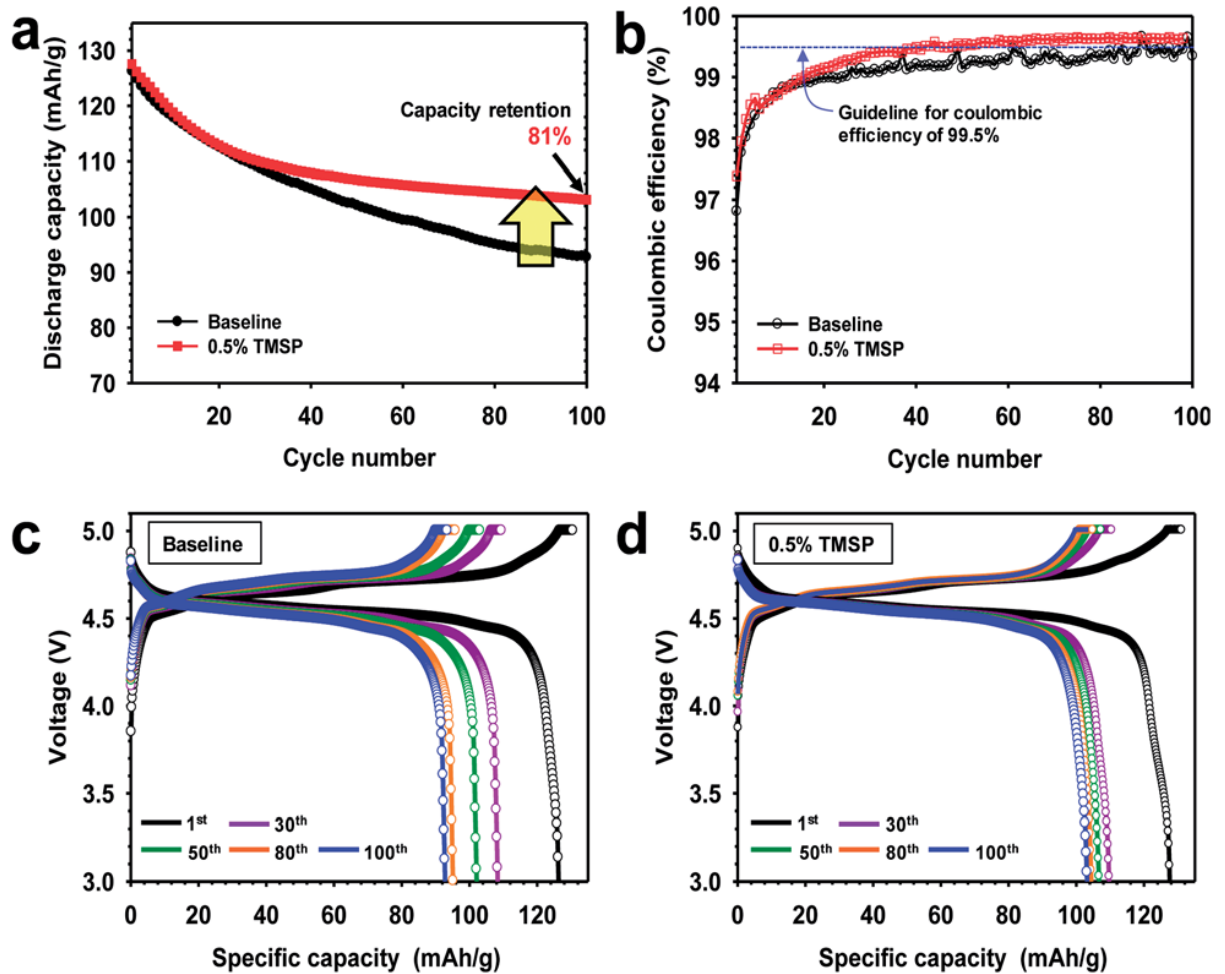


Fig. 2-15 Electrochemical performance of graphite/LiNi_{0.5}Mn_{1.5}O₄ full cells at C/2 and 30 °C when cycled between 3.0 and 5.0 V: (a) cycling stability and (b) coulombic efficiency, charge and discharge curves of the full cell for 1st, 30th, 50th, 80th and 100th cycles in (c) baseline electrolyte and (d) TMSP-added electrolyte. A very high coulombic efficiency (red square) of over 99.5%, which is vital for practical applications, was obtained.

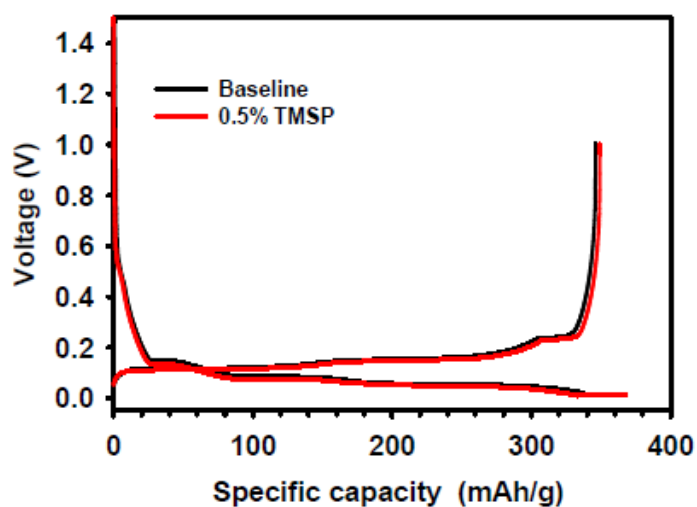


Fig. 2-16 Voltage profiles of the graphite anode with or without 0.5% TMSP for a current density of 35 mA g^{-1} (electrode capacity = 2.55 mAh cm^{-2}) during precycling.

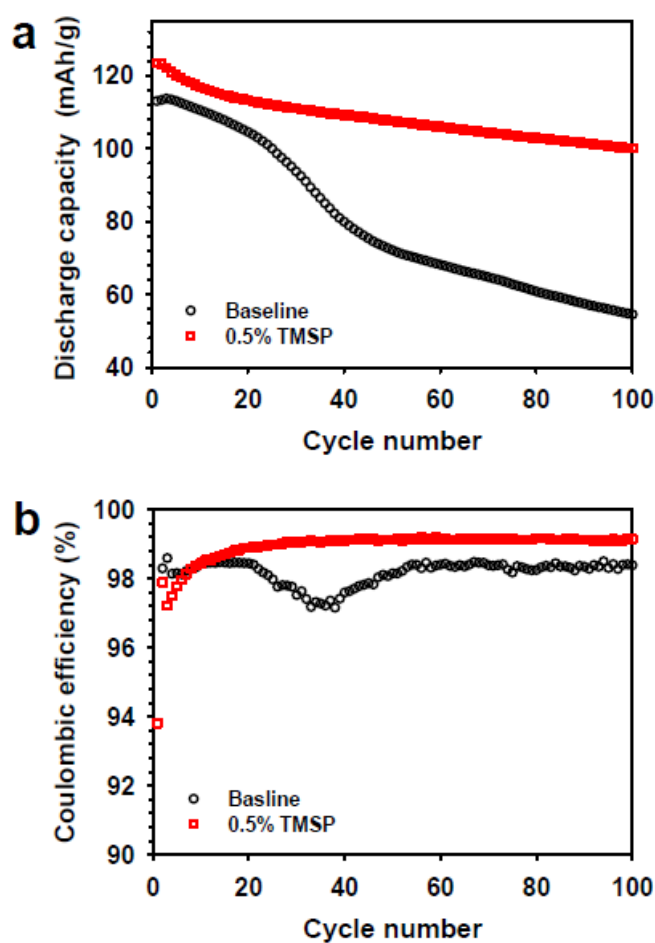


Fig. 2-17 (a) Discharge capacity, (b) Coulombic efficiency of graphite/ $\text{LiNi}_{0.5}\text{Mn}_{1.5}\text{O}_4$ full cells in baseline and TMSP-added electrolytes at 45°C at a rate of $C/2$.

To verify this, the graphite anode from a graphite/LiNi_{0.5}Mn_{1.5}O₄ full cell after 100 cycles was analyzed by EDS measurements. Mn and Ni signals were clearly observed on the graphite anode in a full cell that was cycled during 100 cycles in the baseline electrolyte, whereas the presence of TMSP excluded the peaks assigned to Mn and Ni elements (see Fig. 2-18b and c). This is probably because TMSP eliminated HF from the electrolyte and thereby Mn and Ni dissolution from the cathode was effectively restrained (see Fig. 2-18e). Further evidence, which proves that the Mn and Ni dissolution by HF attack is drastically alleviated in the presence of TMSP, is shown in Fig. 2-18d. It is also possible that the TMSP-derived SEI on the cathode imparts resistance to the metal dissolution under high voltage conditions. Unlike the pristine graphite showing a very clean surface, the graphite anode from a full cell cycled in the baseline electrolyte during 100 cycles revealed a bumpy surface due to nonuniform SEI layers (Fig. 2-18b and e).

It should be noted that metallic Mn and Ni deposited on the surface of the graphite anode lead to a significant decomposition of the electrolyte and result in the formation of thick SEI layers (Fig. 2-18e). On the other hand, the graphite cycled in a TMSP-containing electrolyte did not display the rough surface. Therefore, it can be thought that the TMSP-containing electrolyte effectively suppresses the migration of Mn and Ni ions toward the graphite anode.

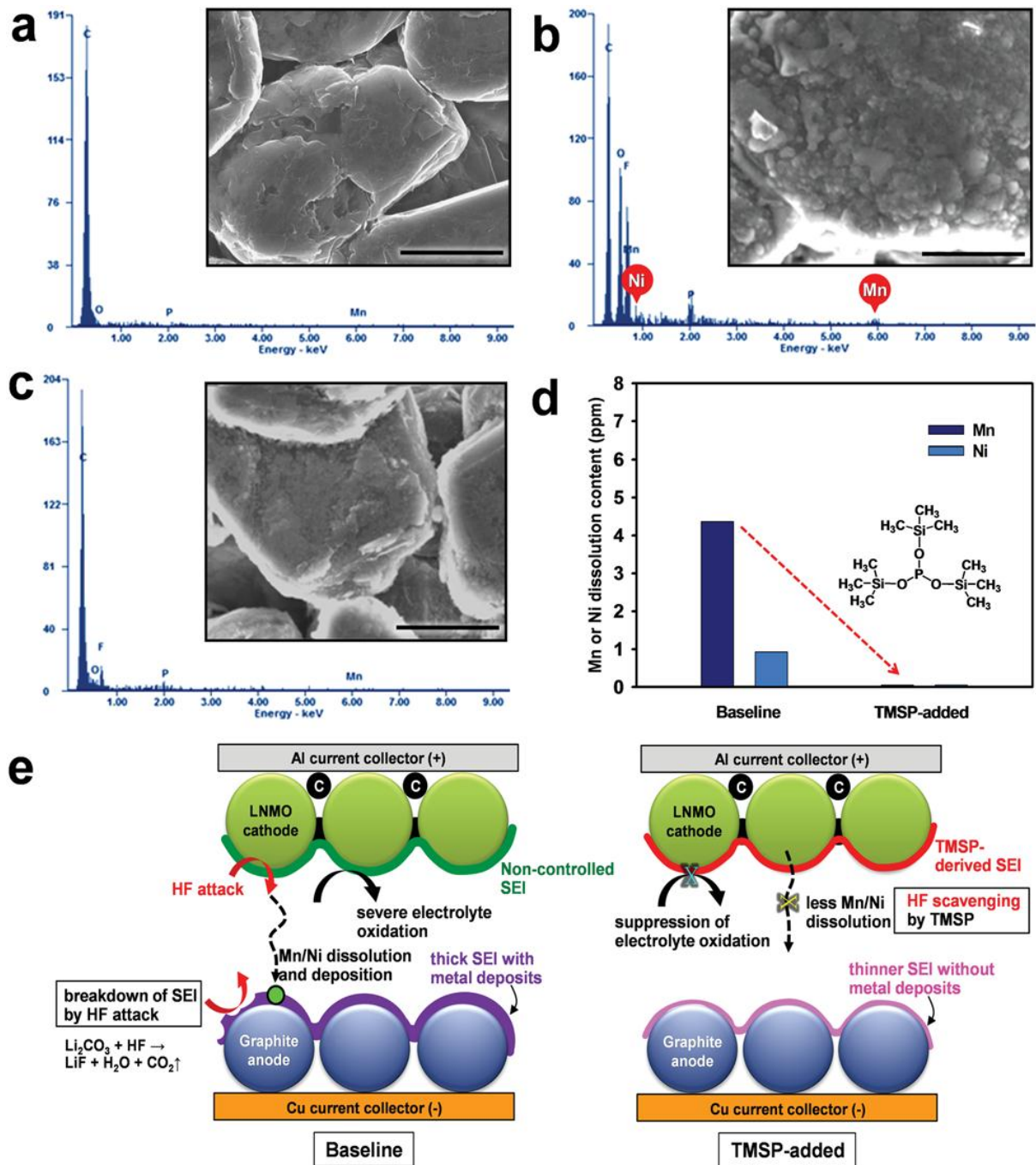


Fig. 2-18 EDS patterns and SEM images of (a) pristine graphite and graphite anodes retrieved from graphite/ $\text{LiNi}_{0.5}\text{Mn}_{1.5}\text{O}_4$ full cells after 100 cycles at 30 °C in (b) baseline electrolyte and (c) TMSP-added electrolyte. Scale bar represents 5 mm. (d) ICP result showing the amount of Mn and Ni dissolution from non-cycled $\text{LiNi}_{0.5}\text{Mn}_{1.5}\text{O}_4$ cathodes in the electrolytes with and without TMSP at 60 °C for 12 h. The use of TMSP inhibited the Mn and Ni dissolution from the pristine cathode. (e) Schematic illustration of unique functions of TMSP in a full cell.

Comparison of the initial charge and discharge profiles of the Li/LiNi_{0.5}Mn_{1.5}O₄ half cells in electrolytes with and without additives at 30 °C is presented in Fig. 2-19. Significant overcharging of the LiNi_{0.5}Mn_{1.5}O₄ cathode took place in a 1% VC-added electrolyte when charged up to 5.0 V; thereby, the initial coulombic efficiency (ICE) of the cathode drastically decreased to 71.2% compared with cells precycled in baseline, and FEC-added and TMSP-added electrolytes. The voltage plateau around 4.85 V and the low ICE of the Li/LiNi_{0.5}Mn_{1.5}O₄ cell with 1% VC could be explained by severe VC decomposition on the high voltage cathode surface at 30 °C.

Moreover, it was clear that the VC additive continuously underwent oxidative decomposition which resulted in a significant oxidative differential capacity at over 4.8 V during 5 cycles at 60 °C (see dQ/dV in Fig. 2-19b). This is because the VC additive is prone to oxidize at a high charge potential of 5.0 V due to its relatively high HOMO energy level, compared to conventional carbonate solvents such as EC (Fig. 2-4). By field-emission scanning electron microscopy (FE-SEM), the cathode cycled in the baseline electrolyte seemed to be partly covered with small particles, whereas the surface film originating from VC decomposition appeared to be discontinuous and relatively thick on the cathode surface after cycling at 60 °C (Fig. 2-20b and c). Although preferential reduction of VC as the most effective additive prior to other electrolyte solvents resulted in a stable SEI on the anode,^{62,63} VC showed the worst oxidation stability toward high voltage cathodes. Moreover, the VC-derived SEI was not maintained during cycling and was appreciably peeled away from the cathode surface, as shown in Fig. 2-20c. To investigate the cathode SEI formed by VC, the surface of the cathode after 5 cycles at 60 °C was examined by ex situ XPS (Fig. 2-21). The C 1s and O 1s XPS spectra clearly showed that VC produced ether (C–O–C) and carboxylate groups as the dominant species in the LiNi_{0.5}Mn_{1.5}O₄ cathode surface layer. Interestingly, peaks that could be assigned to poly(VC), which would generally be observed on the anode, were not detected on the LiNi_{0.5}Mn_{1.5}O₄ cathode cycled in the VC-added electrolyte (see O 1s and C 1s XPS of Fig. 2-21). This implied that VC did not decompose into poly(VC) on the cathode charged up to 5.0 V. Comparing the initial charge and discharge profiles of the LiNi_{0.5}Mn_{1.5}O₄ cathodes in electrolytes with and without a 5% FEC-added electrolyte at 30 °C, there were no significant differences in charge and discharge capacities (Fig. 2-19a). However, the dQ/dV graph obtained during 5 cycles at 60 °C clearly showed that appreciable differential capacity was generated by the severe oxidative decomposition of the FEC-added electrolyte (Fig. 2-19b). It is thought that FEC undergoes considerable oxidative decomposition on the high voltage cathode surface at 60 °C compared to the baseline electrolyte.

Although an FEC-derived surface film was formed on the cathode (see Fig. 2-20), it did not preserve the electrochemical performance of the LiNi_{0.5}Mn_{1.5}O₄ cathode during cycling at 60 °C (Fig. 2-7). The dQ/dV graphs confirmed that the VC and FEC additives were detrimental to the interfacial stability of LiNi_{0.5}Mn_{1.5}O₄ cathodes charged up to 5 V.

The TMSP-added electrolyte exhibited a slightly reduced ICE of 88.0% compared to the baseline electrolyte (88.2%). This was probably because the TMSP decomposition reaction on the cathode resulted in a capacity loss during the first charge and discharge process. Since the HOMO energy (-8.097 eV) of TMSP is higher than that of EC (-11.905 eV) (Fig. 2-4), TMSP is more prone to lose electrons relative to the EC solvent when charged up to 5.0 V. Thus, TMSP oxidation on the $\text{LiNi}_{0.5}\text{Mn}_{1.5}\text{O}_4$ cathode is thought to take place prior to that of other electrolyte components (solvents and salt), forming the cathodic SEI. The characteristics of the SEI formed on the cathode represent a key parameter that influences the kinetics of delithiation–lithiation and the interfacial stability during long-term cycling. Importantly, the $\text{LiNi}_{0.5}\text{Mn}_{1.5}\text{O}_4$ cathode cycled in the TMSP-added electrolyte showed no differential capacity attributed to the oxidative decomposition of the electrolyte when charged up to 5.0 V at 60 °C (see the TMSP-added sample in Fig. 2-19b). Moreover, the cathode cycled in the TMSP-added electrolyte at 60 °C had a very clean and smooth surface (Fig. 2-20). This implied that the TMSP-derived SEI formed during precycling was maintained and effectively alleviated further electrolyte decomposition during cycling at 60 °C. The distinction between the TMSP-added and other electrolytes can be ascribed to the differences in the electrochemical natures of the SEIs formed on the high voltage cathodes.

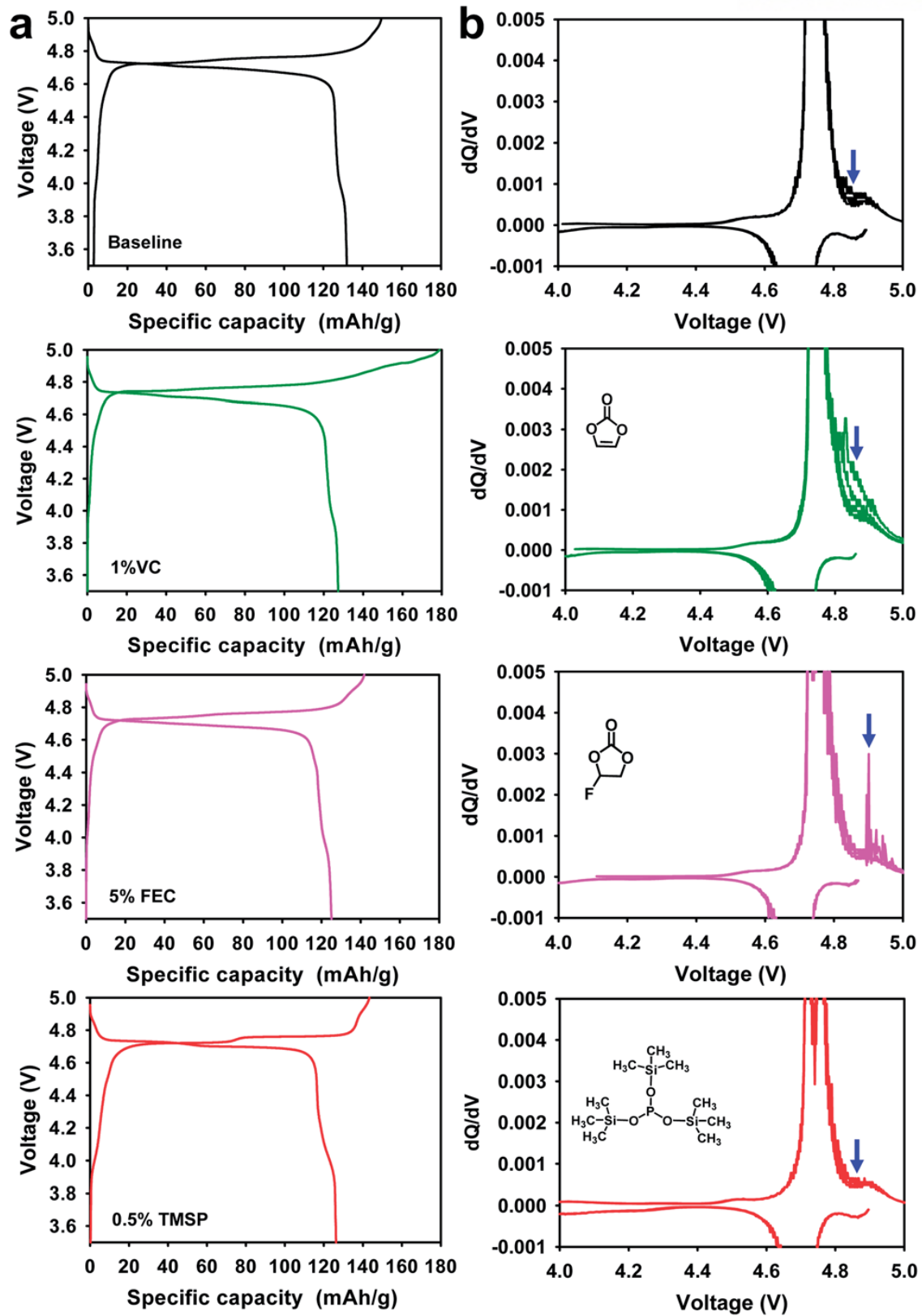


Fig. 2-19 (a) Initial charge and discharge profiles at 30 °C and (b) dQ/dV graphs of 5 V-class $\text{LiNi}_{0.5}\text{Mn}_{1.5}\text{O}_4$ cathodes in various electrolytes during 5 cycles at 60 °C after initial cycling at 30 °C.

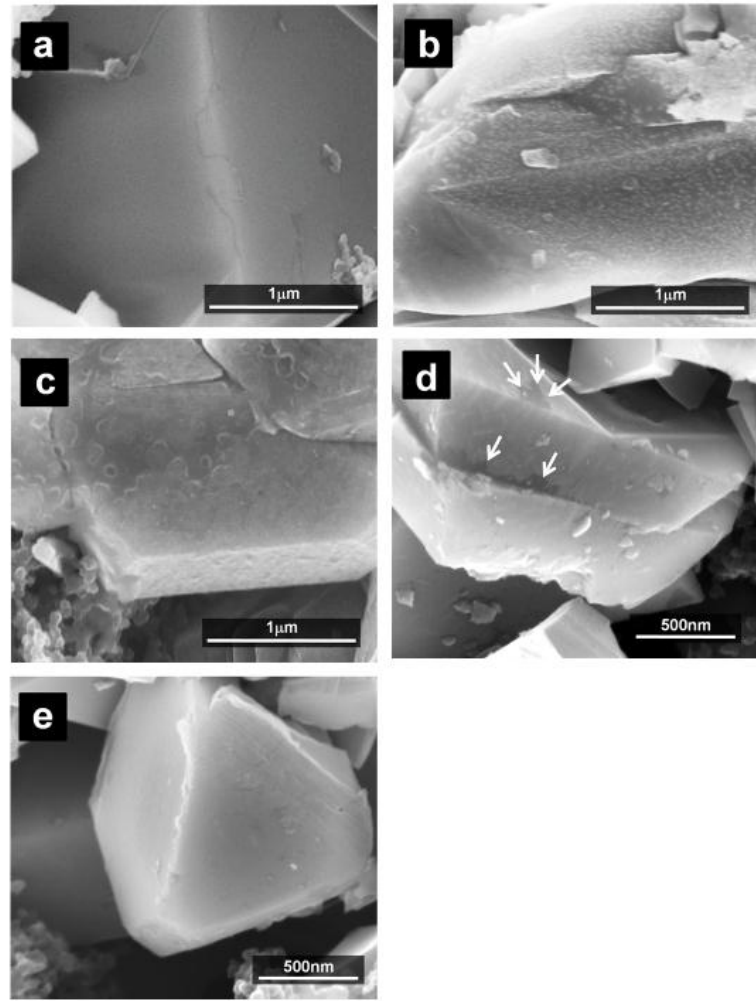


Fig. 2-20 FE-SEM images of the $\text{LiNi}_{0.5}\text{Mn}_{1.5}\text{O}_4$ cathodes after 5 cycles at 60°C : (a) pristine cathode, (b) baseline electrolyte, (c) 1% VC-added, (d) 5% FEC-added, and (e) 0.5% TMSPadded.

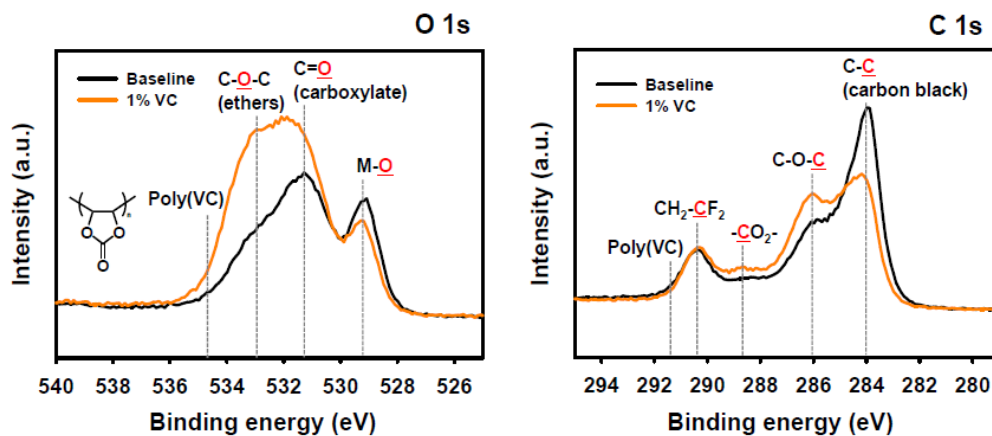


Fig. 2-21 O 1s and C 1s XPS spectra of the $\text{LiNi}_{0.5}\text{Mn}_{1.5}\text{O}_4$ cathodes cycled in baseline and VC-added electrolytes during 5 cycles at 60°C .

To verify the superior anodic stability of the TMSP-added electrolyte, the leakage current of Li/ LiNi_{0.5}Mn_{1.5}O₄ cells was monitored at a constant charging voltage of 5.0 V for 5 h. The baseline electrolyte showed a much larger leakage current, which indicated significant oxidative decomposition of the electrolyte, whereas the presence of TMSP greatly reduced the leakage current (Fig. 2-22a). Linear sweep voltammetry (LSV) results confirmed that the anodic stability of the electrolyte could be improved by TMSP (Fig. 2-22b). These results suggested that the TMSP-derived SEI formed on the cathode surface helped the electrolyte tolerate a high voltage of 5.0 V.

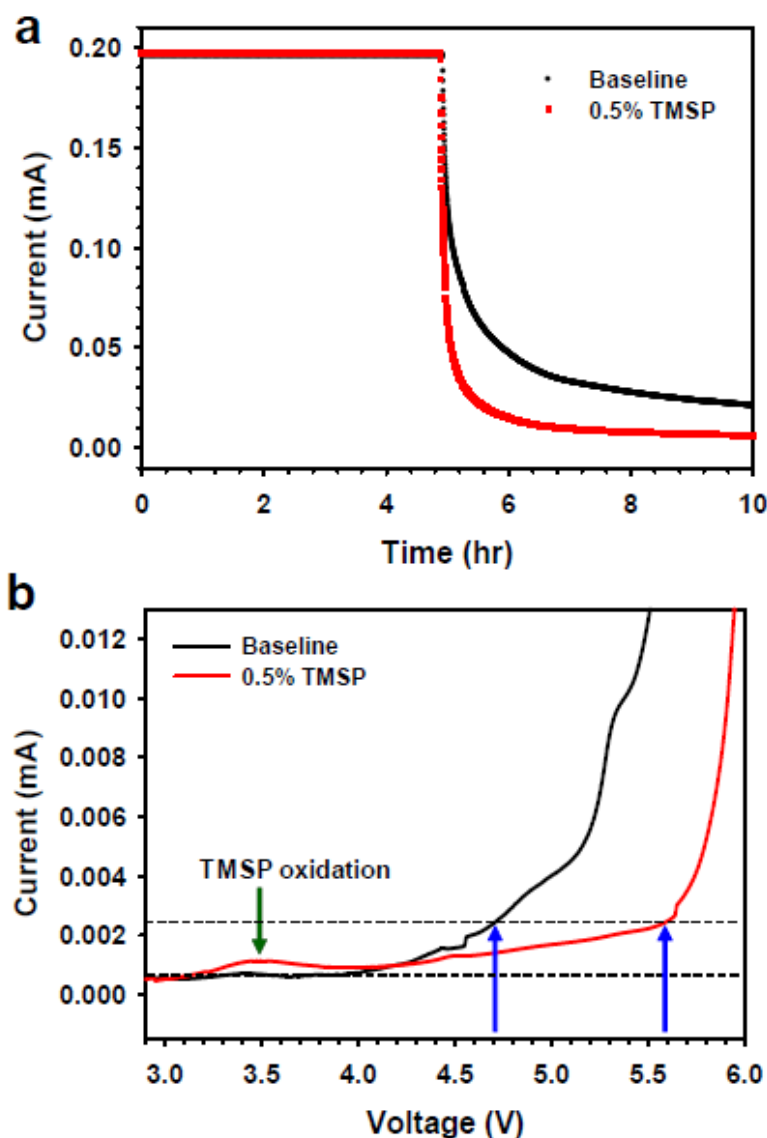


Fig. 2-22 (a) Potentiostatic profiles of Li/ LiNi_{0.5}Mn_{1.5}O₄ half cells maintained at charging voltage of 5.0 V after charging up to 5.0 V at 30 °C. (b) Linear sweep voltammetry of electrolytes with and without 0.5% TMSP additive. Stainless steel was used as a working electrode and the scan rate was 1 mV/s.

2.3.2 Comparison with phosphite-containing electrolytes

Herein, to convince the practical impact and additional function of organophosphorous-based additives, we present progressive study comparing TMSP with other additives commonly retaining phosphite core. In addition, from an analysis of surface chemistry of SEI layers on the high voltage cathode, we can find similar components of SEI layers formed by various phosphite-added electrolytes via ex situ X-ray photoelectron spectroscopy (XPS), and propose its common functions which eliminate HF and alleviate decomposition of LiPF_6 by hydrolysis via nuclear magnetic resonance (NMR).

Fig. 2-23 indicated various candidates as an oxidative additive for high voltage $\text{LiNi}_{0.5}\text{Mn}_{1.5}\text{O}_4$ cathode. Phosphite-based additives which can be used as solid electrolyte interphase (SEI) layer formation due to higher highest occupied molecular orbital (HOMO) energy level than carbonate-based solvent identically include three P-O moieties, but have different groups such as methyl, phenyl, 2,2,2-fluoroethyl, silyl group (Fig. 2-23).

Voltage profile and initial coulombic efficiency (ICE) of $\text{Li}/\text{LiNi}_{0.5}\text{Mn}_{1.5}\text{O}_4$ cathodes with or without additives were presented in Fig. 2-24 during precycling. A plateau at 4.0V attributed to the $\text{Mn}^{3+}/\text{Mn}^{4+}$ redox couple was clearly observed, and the high-voltage plateau around 4.7-4.75V due to $\text{Ni}^{2+}/\text{Ni}^{3+}$ and $\text{Ni}^{3+}/\text{Ni}^{4+}$ redox couples also was expressed in all of the sample. The charge/discharge coulombic efficiency in tris(2,2,2-trifluoroethyl)phosphite (TFEP) and tris(trimethylsilyl)phosphite (TMSP) increased over 90%, but trimethylphosphite(TMP) and triphenylphosphite(TPP) showed lower value than baseline electrolyte (baseline electrolyte $\approx 88\%$, with 0.5 wt.% TMP $\approx 83\%$, with 0.5 wt.% TPP $\approx 55\%$, with 0.5 wt.% TFEP $\approx 90\%$, with 0.5 wt.% TMSP $\approx 92\%$).

This change of coulombic efficiency relates to behavior of additives which oxidized on surface of cathode during first charge/discharge process. Generally, oxidative additive decreases coulombic efficiency at first cycle because additive having the highest HOMO level in electrolyte easily prefers to be decomposed and total consumed electrons will be increased. But if SEI layer formed by decomposition of oxidative additive during first charge process alleviated additional decomposition of electrolyte, value of initial coulombic efficiency would indicate different character compared with baseline electrolyte.

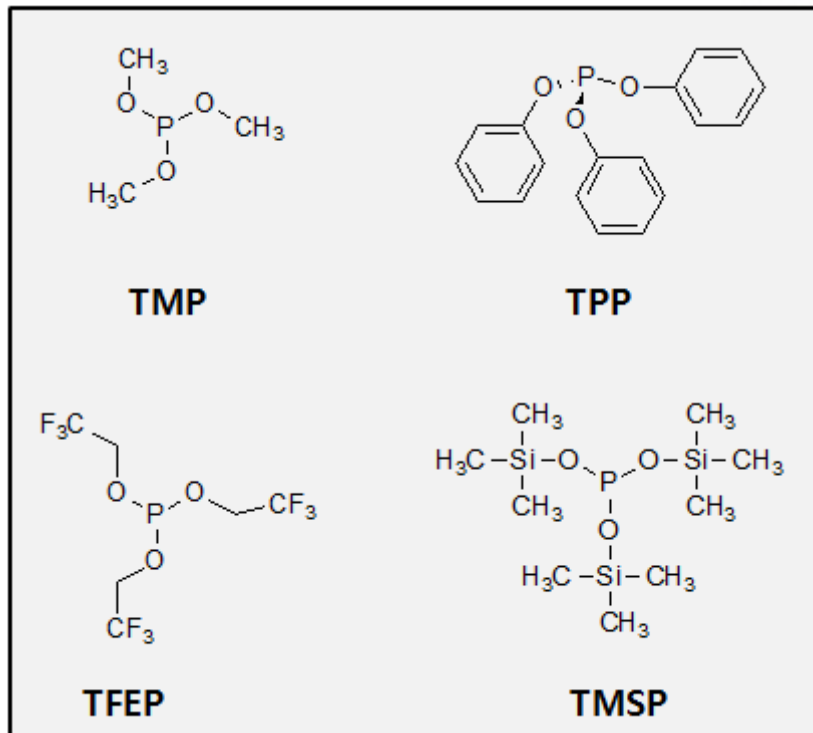


Fig. 2-23 Molecular structures of various phosphite-containing additives.

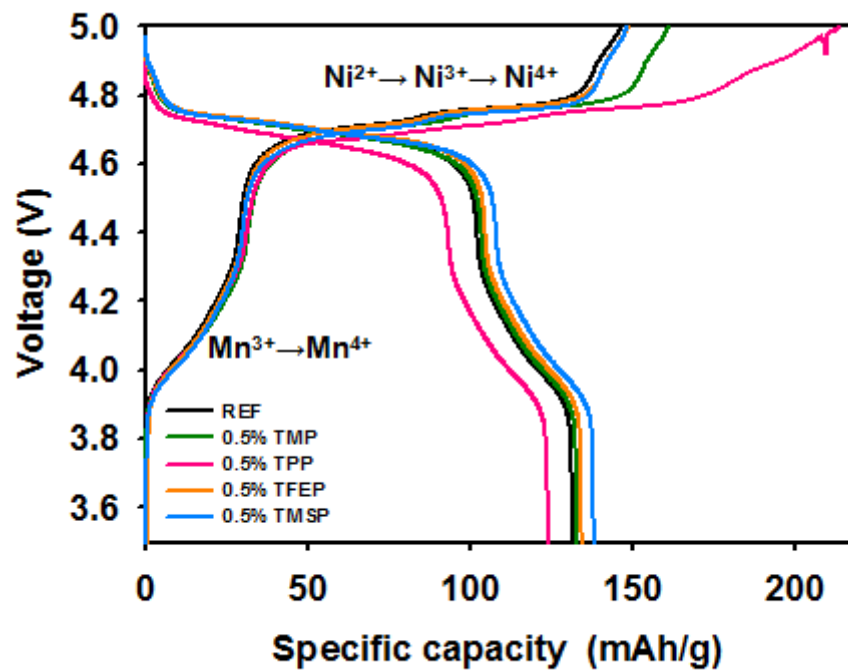


Fig. 2-24 The voltage profiles of $\text{LiNi}_{0.5}\text{Mn}_{1.5}\text{O}_4/\text{Li}$ cell in EC/EMC/DMC 1.0M LiPF_6 without and with 0.5wt% additive.

To investigate the anodic stability of phosphate-based electrolytes at high voltage circumstance, the leakage current of Li/LiNi_{0.5}Mn_{1.5}O₄ cell were monitored at a constant voltage of 5.0 V for 10 h. The leakage current originated by decomposition of electrolyte because of severe oxidative atmosphere showed superior anodic stability of TMSP-added electrolyte and harmful result in TPP-added electrolyte (Fig. 2-25a). Galvanostatic intermittent titration technique (GITT) result confirmed that polarization of TPP-based electrolyte which represented by IOCV-CCVI exhibited higher resistance than the others. The rest of cells including various electrolytes were no significant difference of polarization (Fig. 2-25b). These results suggested that phosphite-derived SEI layer formed on cathode surface except for TPP-based electrolyte helped electrolytes to tolerate at high voltage of 5.0 V.

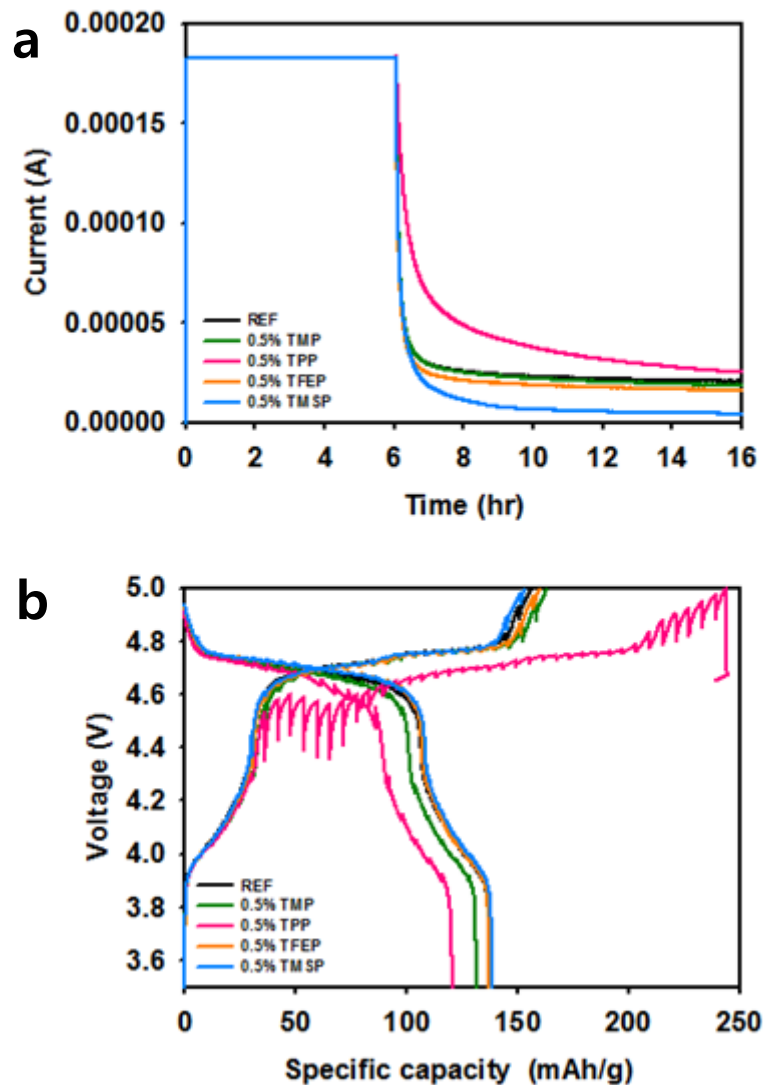


Fig. 2-25 (a) Potentiostatic profiles of $\text{LiNi}_{0.5}\text{Mn}_{1.5}\text{O}_4/\text{Li}$ half cells maintained at charging voltage of 5.0V after charged up to 5.0V at 30 °C, (b) charge and discharge curves by galvanostatic intermittent titration technique (GITT)

The galvanostatic electrochemical cycling performance of $\text{Li}/\text{LiNi}_{0.5}\text{Mn}_{1.5}\text{O}_4$ cells containing diverse phosphite-additives was presented in Fig. 2-26. The cells were cycled at 0.5 C under constant applied current at the range between 3.5 V and 5 V during 100 cycles at 30 °C and 60 °C. Because cycling performance containing with and without diverse phosphite-additives seriously did not be affected at room temperature, significant effects of cycle performance and columbic efficiency (CE) were no observed in Fig. 2-26b. Its discharge capacity retention of the cells reached over 90 % after 100 cycles at 30 °C (baseline electrolyte \approx 94 %, with 0.5 wt.% TMP \approx 97 %, with 0.5 wt.% TPP \approx 92 %, with 0.5 wt.% TFEP \approx 95 % , with 0.5 wt.% TMSP \approx 95 %) in Fig. 4a. However, the cell cycled in baseline electrolyte showed rapidly decreased columbic efficiency after 15 cycles at 60 °C in Fig. 2-26c. This phenomenon which indicated sharp drop of columbic efficiency from 96 % to 90 % could be described as SEI lay formed by baseline electrolyte on $\text{LiNi}_{0.5}\text{Mn}_{1.5}\text{O}_4$ cathode during precycling couldn't maintain its nature due to severe condition of high temperature. On the other hand, the phenomenon cycled in various phosphite-added electrolytes except for TPP-added electrolyte was disappeared during 200 cycles and exhibited approximately 1.5% improved columbic efficiency, compare to baseline electrolyte (Fig. 2-26d). It revealed that SEI layer modified by TMP, TFEP, TMSP was more stable at elevated temperature and robust to suppress severe electrolyte decomposition happened inevitably under oxidative condition. Resultingly, SEI layer formed by baseline electrolyte is more and more stacked by undesirable byproduct and consumes active Li^+ ion as cycle goes on.

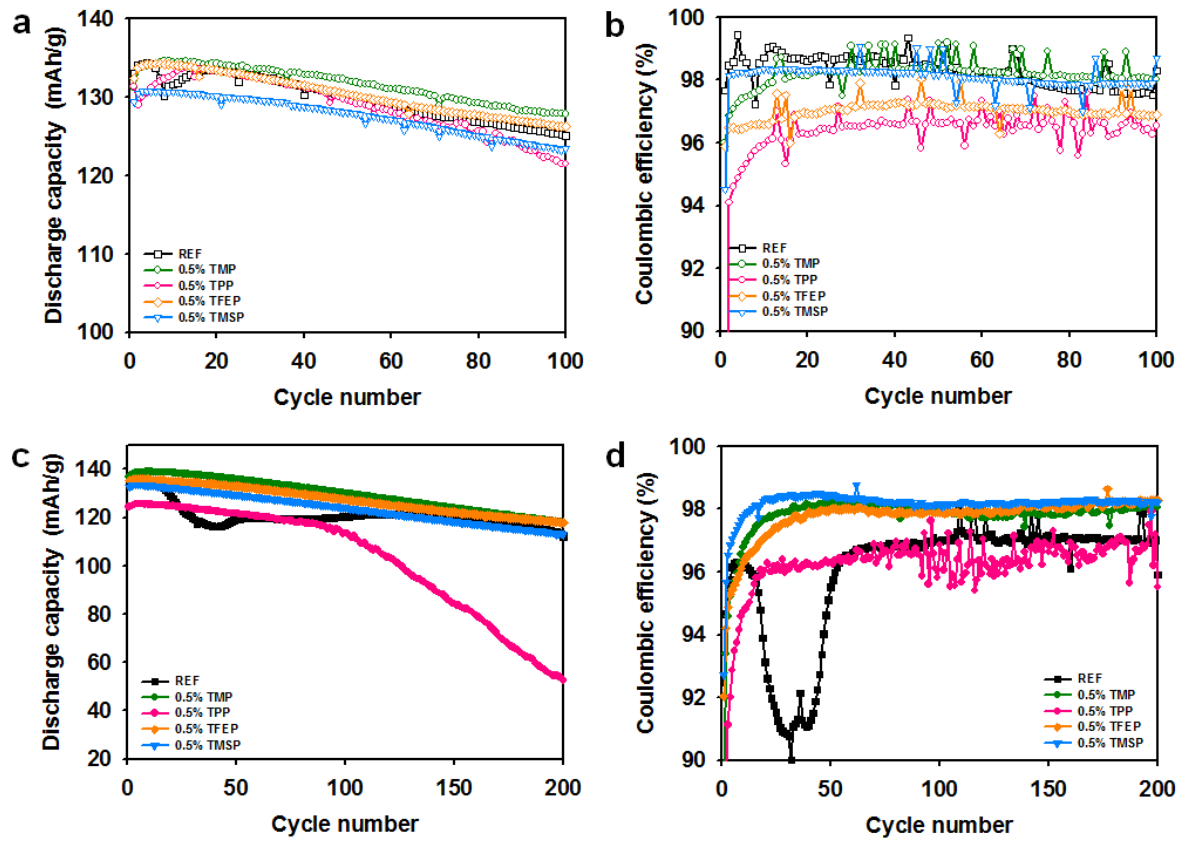


Fig. 2-26 Electrochemical performance of $\text{LiNi}_{0.5}\text{Mn}_{1.5}\text{O}_4$ cathodes at $C/2$ when cycled between 3.5 and 5.0V: (a) Cycling stability at 30°C and (b) coulombic efficiency at 30°C. (c) Cycling stability at 60°C and (d) coulombic efficiency at 60°C.

To find change of $\text{LiNi}_{0.5}\text{Mn}_{1.5}\text{O}_4$ cathodes surface chemistry developed by diverse phosphite-added electrolytes, XPS analysis was evaluated and compared with each cell after precycling at 30 °C. Fig. 2-27 showed F 1s spectra and clearly exhibited peak assigned to P-F and LiF on cathode surface, and the LiF peak of cycled in baseline electrolyte and four phosphite-added electrolytes certainly shown with distinct tendency that phosphite-added electrolytes commonly indicated a much weaker LiF peak caused hydrolysis of LiPF_6 and reaction between HF and Li ion leading severe loss of active Li^+ ion than baseline electrolyte. The P 2p peak assigned to Li_xPF_y (F-P) and $\text{Li}_x\text{PF}_y\text{O}_z$ (F-P-O) from cycled $\text{LiNi}_{0.5}\text{Mn}_{1.5}\text{O}_4$ cathodes surface after precycling also were shown in Fig. 2-27. The peak assigned to $\text{Li}_x\text{PF}_y\text{O}_z$ (F-P-O) from SEI formed by TMSP-added electrolyte was surprisingly increased, compare to other cells. Increased P 2p peak signified the SEI formed by TMSP-additive was made by different way to decompose during precycling. This needs to be further investigated. Additionally, whether TMSP took part in SEI formation, we accepted subsidiary clue throughout Si 2p peak at 102 eV assigned Si-O peak in Fig. 2-27.

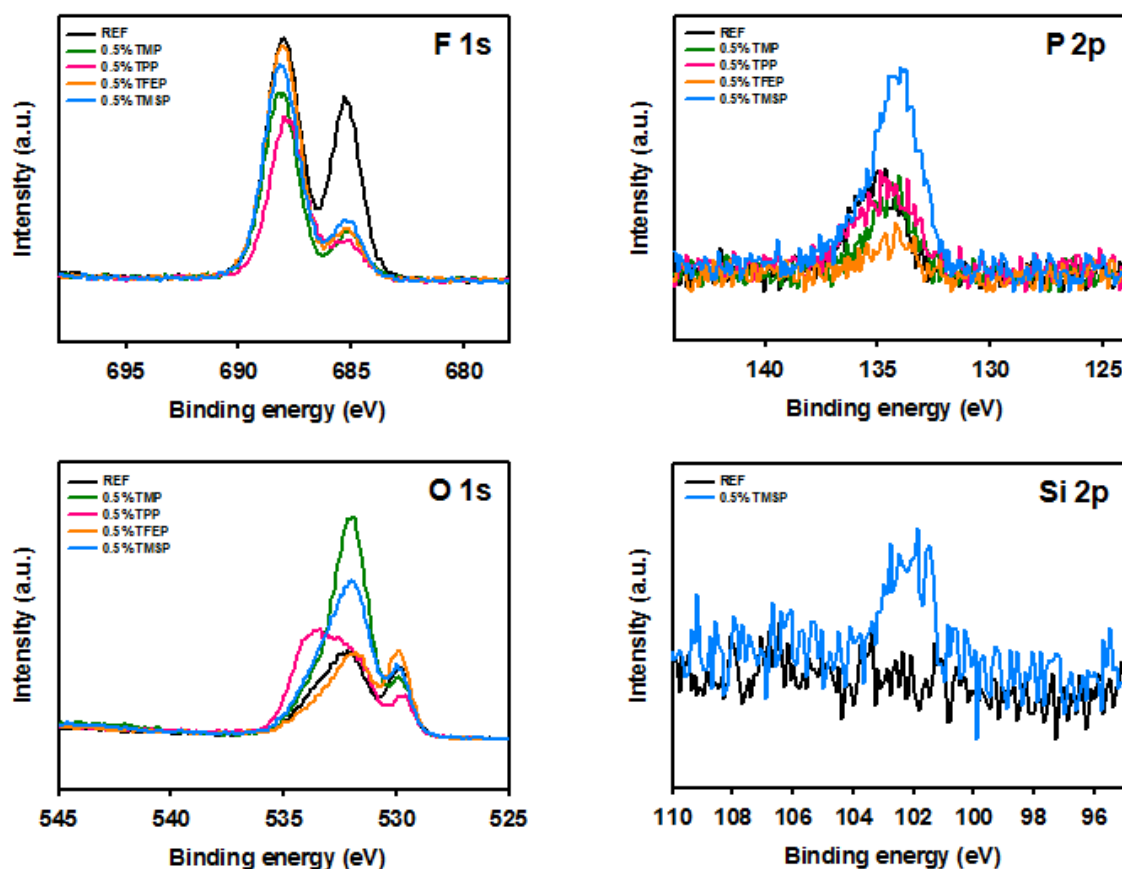
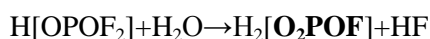
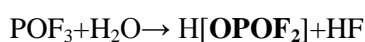
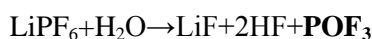


Fig. 2-27 XPS spectra of the $\text{LiNi}_{0.5}\text{Mn}_{1.5}\text{O}_4$ cathodes after precycling at 30 °C.

Whether phosphite-additives eliminate HF produced from the LiPF₆-based electrolyte, 5 vol% water was added to baseline and phosphite-added electrolytes and the outputs were stored in NMR tube during 22 h at room temperature and the resulting solutions finally were analyzed by ¹⁹F and ³¹P NMR (Fig. 2-28). Hydrolysis reaction of LiPF₆ salt can be represented from following reaction formula :

Hydrolysis reactions of LiPF₆ salt : (1)



P-F bond of LiPF₆ salt was prone to hydrolysis if a small amount of water remains in assembled cell. HF produced by hydrolysis of LiPF₆ salt constantly attacks on LiNi_{0.5}Mn_{1.5}O₄ cathodes surface leading to Mn dissolution and trace water increases LiF as SEI component on the cathode, as depicted in reaction formula (1).⁵⁶⁻⁵⁸ The difference of ¹⁹F NMR spectrum between baseline and phosphite-added electrolytes was indicated at -154.7 ppm corresponded to the characteristic resonance of HF. When phosphite-additives were inserted into baseline electrolyte solutions, intensity of HF remarkably was decreased due to direct reaction between HF and phosphite-additives (Fig. 2-28). This result was persuasive evidence that additives having phosphite core commonly help to remove HF in comparison with baseline electrolyte and dissolution of transition metal ions (Mn and Ni) are expected to be decreased, also suppress to LiF formation on the cathode produce by consume Li ion in accordance with XPS data in Fig. 2-27.

Another effect of phosphite-additives which showed function of HF removal was present in fig. 2-29. It showed typical resonance produced by hydrolysis of LiPF₆ salt such as PO₂F₂⁻ and PO₃F²⁻ from identical sample presented in Fig. 2-29. This revealed that all phosphite-additives effectively alleviated create of PO₂F₂⁻ and PO₃F²⁻ which generated by hydrolysis contrary to baseline electrolyte ; these weaker peak mean that phosphite-additives can remove HF but also eliminate water in the cell by direct reaction. TMSP-added electrolyte showed the highest good functions which scavenge HF and prevent hydrolysis of LiPF₆ salt among all phosphite-added electrolytes.⁵⁹⁻⁶¹

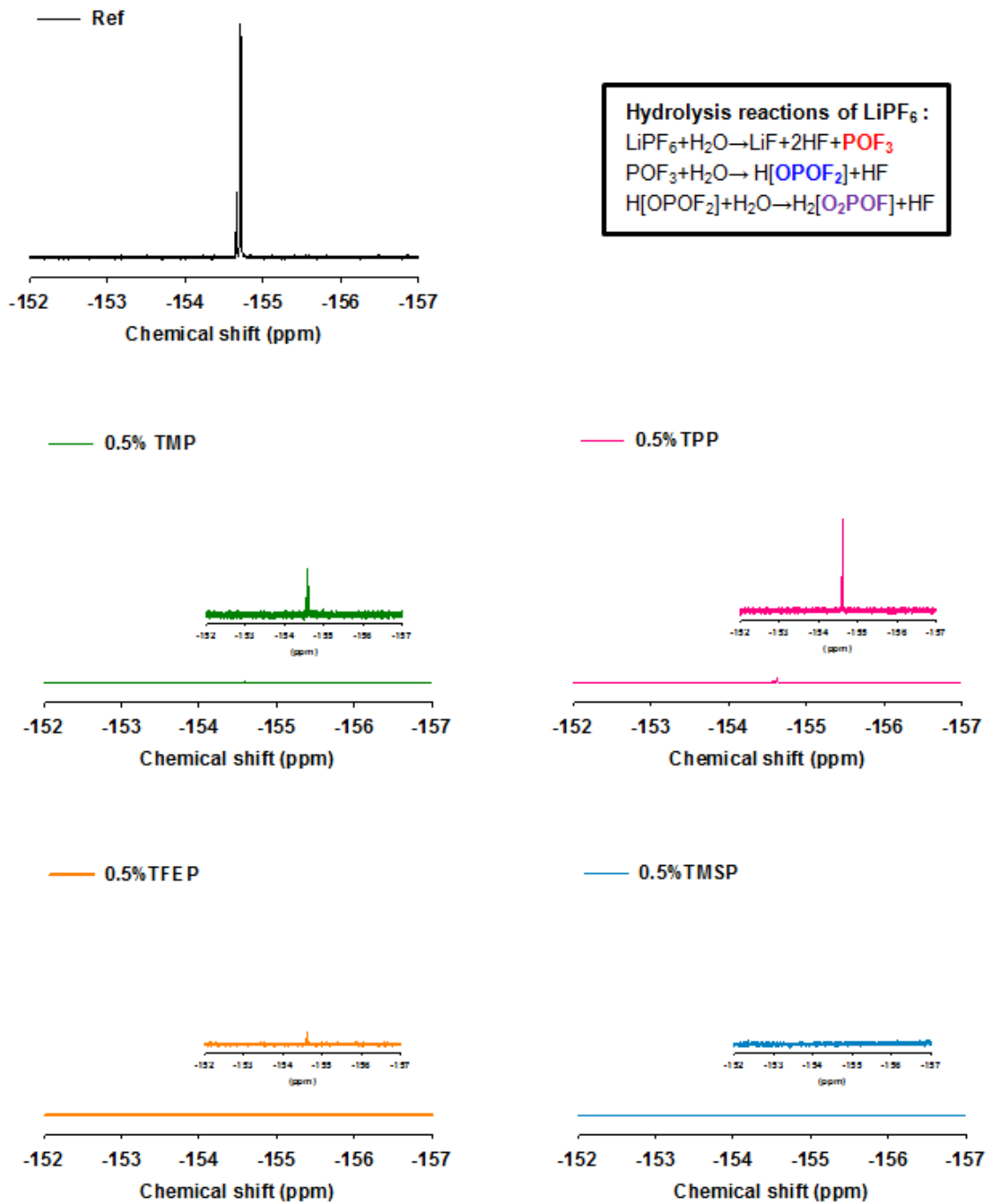


Fig. 2-28 ^{19}F NMR spectra of the electrolyte with and without additive after hydrolysis tests at room temperature. HF was completely removed from the electrolyte in presence of phosphite-containing additives.

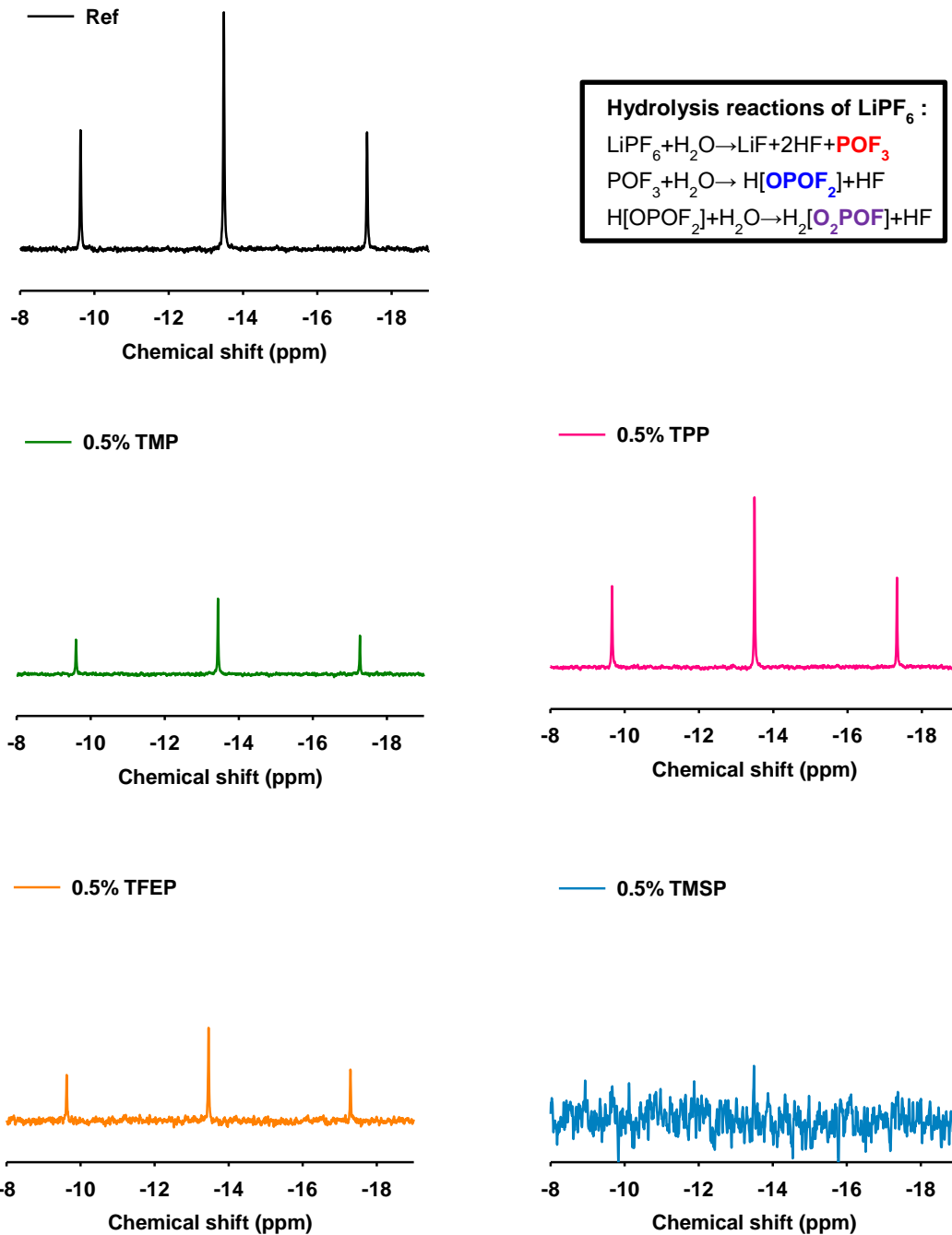


Fig. 2-29 ¹⁹P NMR spectra of the electrolyte with and without additive after hydrolysis tests at room temperature.

To investigate the suitability of phosphite-derived SEI for facilitating charge transfer at cathode surface, rate capability was implemented by computer-controlled battery measurement system at different C-rate from 0.5 C to 5 C during discharge and same charge rate at 0.5 C (Fig. 2-30). Phosphite-added electrolytes excluded TPP-added electrolyte showed better discharge capacity than baseline electrolyte. Among them TMSP-added electrolyte clearly exhibited a superior rate capability. The $\text{LiNi}_{0.5}\text{Mn}_{1.5}\text{O}_4$ cathode with TMSP additive delivered a remarkable discharge capacity (130 mAh/g) at a very high current density (600 mA/g, corresponding 5 C) compare to baseline electrolyte (120 mAh/g) at 30 °C (with 0.5 wt.% TMP \approx 123 mAh/g, with 0.5 wt.% TPP \approx 108 mAh/g, with 0.5 wt.% TFEP \approx 123 mAh/g). However, the cell cycled in TPP-added electrolyte showed relative rapid capacity fading as a function of the applied current density because This result implied that various phosphite-additives developed respective unusual SEI and resistance of SEI affected electrochemical properties. So, we speculated that TMP, TFEP, TMSP-derived compact SEI showed good ion permeability and inhibited oxidative decomposition of electrolyte also were protected by HF made from hydrolysis of LiPF_6 -based electrolyte. HF attack on $\text{LiNi}_{0.5}\text{Mn}_{1.5}\text{O}_4$ cathodes surface leads to fatal problem related to Mn^{2+} dissolution limiting the commercialization of high voltage $\text{LiNi}_{0.5}\text{Mn}_{1.5}\text{O}_4$ cathodes, because Mn^{2+} ion dissolved into electrolytes causes severe capacity fading and provoke unwanted side reaction. To verify disparity of the interfacial resistance of cathode formed by various additives after precycling, electrochemical impedance spectroscopy (EIS) was investigated and interfacial resistance involving R_{sei} component was smaller for the cell in phosphite-added electrolytes except TPP-added electrolytes corresponding with rate capability data (Fig. 2-31).

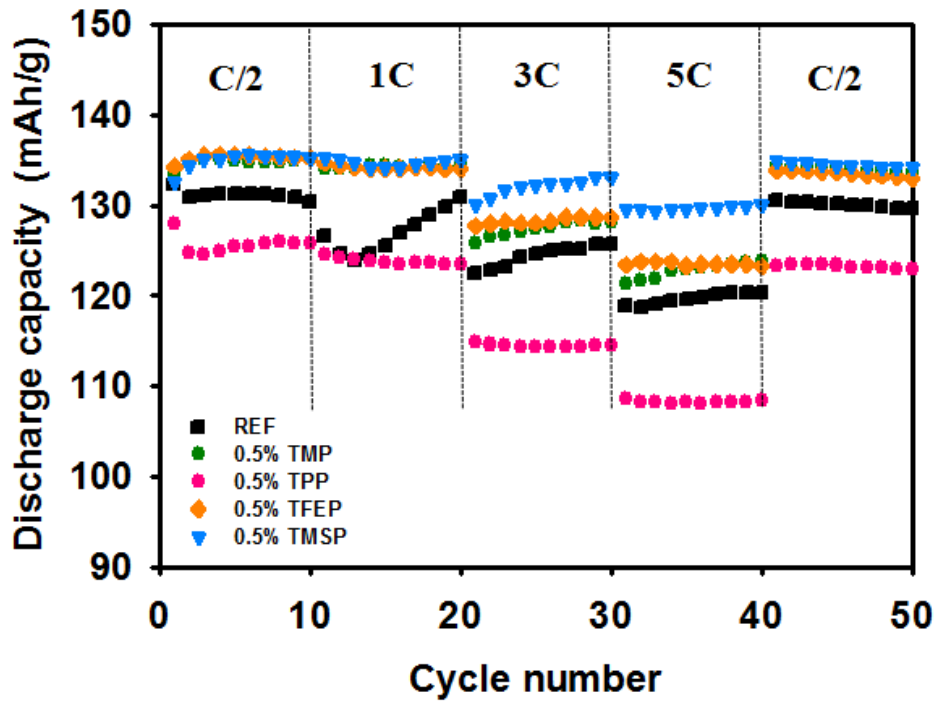


Fig. 2-30 Rate capability at different C rates depending on additive.

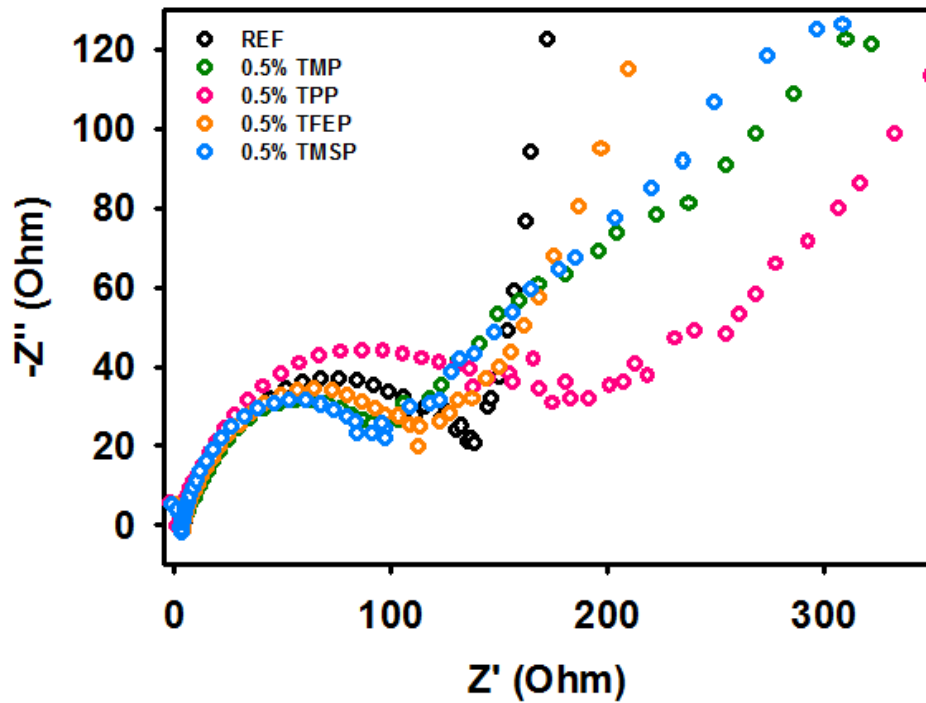


Fig. 2-31 AC impedance spectra of $\text{LiNi}_{0.5}\text{Mn}_{1.5}\text{O}_4$ after precycle in electrolyte with and without additives.

To have a further comparison of the storage ability, delithiated- $\text{LiNi}_{0.5}\text{Mn}_{1.5}\text{O}_4$ cathodes were stored at 60°C and discharge capacity retention of each cell was implemented after open circuit voltage (OCV) was measured during 6 days (Fig 2-32). Resultingly, cell containing TMSP-additive showed the highest value of OCV, compared to other cells (baseline electrolyte : 4.31V, with 0.5 wt.% TMP : 4.23V, with 0.5 wt.% TPP : 4.13, with 0.5 wt.% TFEP : 4.25, with 0.5 wt.% TMSP : 4.69) in fig. 2-32a. This result which was regarded as self-discharge indicates instability of delithiated- $\text{LiNi}_{0.5}\text{Mn}_{1.5}\text{O}_4$ cathodes and electrolyte decomposition. So, the cell containing TMSP-additive implies that SEI formed by TMSP maintains structure of cathode and had more stable character than other things against to electrolyte decomposition, linked to fig. 2-32b which showed result of discharge capacity retention.

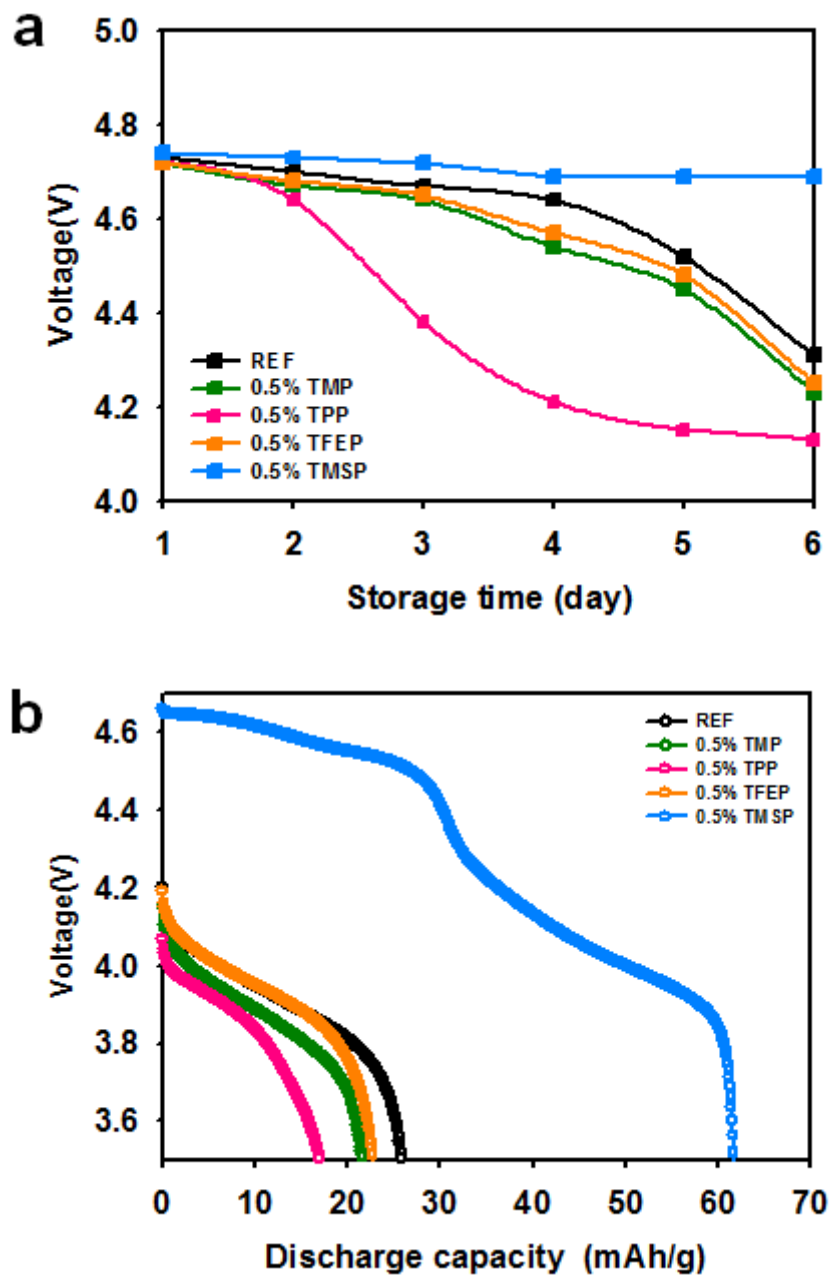


Fig. 2-32 Properties in storage test at 60 °C: (a) representation of OCV drop of Li/LiNi_{0.5}Mn_{1.5}O₄ half-cell, (b) discharge capacity retention after storage during 6 days.

2.4 Conclusion

First, our group reported improved electrochemical performance of Li/LNMO half cell and Graphite/LNMO full cell by using new additive having phosphite-core. Tris(trimethylsilyl) phosphite (TMSP) showed very promising materials for additive, because solid electrolyte interface (SEI) layer formed by TMSP which has higher highest occupied molecular orbital (HOMO) than carbonate-based electrolyte indicated faster charge transfer at the cathode surface and inhibited direct contact of electrolyte with the high-voltage cathode, thus, efficiently reduced continuous oxidative decomposition of electrolyte under repeated cycling at elevated temperatures and high voltages, and to mitigate Mn/Ni dissolution from $\text{LiNi}_{0.5}\text{Mn}_{1.5}\text{O}_4$ cathode. Furthermore, by analyzing XPS data after cycling, we found SEI layer formed by TMSP was composed of inorganic phosphorous-based species with organic ether and carboxylate/carbonate moieties, and the LIF produced by decomposition of LiPF_6 was significantly reduced. In other word, TMSP additive alleviated the decomposition of LiPF_6 by hydrolysis, and the function of TMSP additive-eliminating HF catalyzing the decomposition of electrolyte was elucidated by ^{19}F and ^{31}P NMR studies.

Second, by progressive study comparing TMSP with other additives commonly retaining phosphite core, we try to convince the practical impact and additional function of phosphite-type additive. Through this study, we can find similar components of SEI layers formed by various phosphite-added electrolytes by an analysis of surface chemistry of SEI layers on the high voltage cathode via ex situ X-ray photoelectron spectroscopy (XPS). In addition, we proposed its common functions which eliminate HF and alleviate decomposition of LiPF_6 by hydrolysis via nuclear magnetic resonance (NMR). It is efficient to design suitable electrolyte systems for high-voltage $\text{LiNi}_{0.5}\text{Mn}_{1.5}\text{O}_4$ cathode and we expect other additional study will be conducted to improve electrochemical performance.

References

1. Choi, N. S.; Chen, Z.; Freunberger, S. A.; Ji, X.; Sun, Y. K.; Amine, K.; Yushin, G.; Nazar, L. F.; Cho, J.; Bruce, P. G., Challenges Facing Lithium Batteries and Electrical Double-Layer Capacitors., *Angewandte Chemie International Edition* **2012**, 51 (40), 9994.
2. Tarascon, J.-M.; Armand, M., Issues and challenges facing rechargeable lithium batteries. *Nature* **2001**, 414 (6861), 359.
3. Bruce, P. G.; Freunberger, S. A.; Hardwick, L. J.; Tarascon, J.-M., Li-O₂ and Li-S batteries with high energy storage. *Nature materials* **2011**, 11 (1), 19.
4. Dunn, B.; Kamath, H.; Tarascon, J.-M., Electrical energy storage for the grid: A battery of choices. *Science* **2011**, 334 (6058), 928-935.
5. Etacheri, V.; Marom, R.; Elazari, R.; Salitra, G.; Aurbach, D., Challenges in the development of advanced Li-ion batteries: a review. *Energy & Environmental Science* **2011**, 4 (9), 3243.
6. O. K. Park, Y. , S. Lee, H.-C. Yoo, H.-K. Song and J. Cho, Who will drive electric vehicles, olivine or spinel? *Energy & Environmental Science* **2011**, 4, 1621.
7. T. Ohzuku, K. Ariyoshi and S. Yamamoto, Synthesis and characterization of Li[Ni_{1/2}Mn_{3/2}]O₄ by two-step solid state reaction. *J. Ceram. Soc. Jpn.* **2002**, 110, 501.
8. Q. Zhong, A. Bonakdarpour, M. Zhang, Y. Gao and J. R. Dahn, Synthesis and electrochemistry of LiNi_xMn_{2-x}O₄. *J. Electrochem. Soc.* **1997**, 144, 205.
9. Y. Idemoto, H. Narai and N. Koura, Crystal structure and cathode performance dependence on oxygen content of LiMn_{1.5}Ni_{0.5}O₄ as a cathode material for secondary lithium batteries. *J. Power Sources* **2003**, 119.
10. K. Ariyoshi, Y. Iwakoshi, N. Nakayama and T. Ohzuku, Topotactic two-phase reactions of Li[Ni_{1/2}Mn_{3/2}]O₄ (P4(3)32) in nonaqueous lithium cells. *J. Electrochem. Soc.* **2004**, 151, A296.
11. B. J. Hwang, Y. W. Wu, M. Venkateswarlu, M. Y. Cheng and R. Santhanam, Influence of

synthesis conditions on electrochemical properties of high-voltage $\text{Li}_{1.02}\text{Ni}_{0.5}\text{Mn}_{1.5}\text{O}_4$ spinel cathode material., *J. Power Sources* **2009**, 193, 828.

12. E.-S. Lee, K.-W. Nam, E. Hu and A. Manthiram, Influence of Cation Ordering and Lattice Distortion on the Charge-Discharge Behavior of $\text{LiMn}_{1.5}\text{Ni}_{0.5}\text{O}_4$ Spinel between 5.0 and 2.0 V. *Chem. Mater.* **2012**, 24, 3610–3620.

13. J. Song, D. W. Shin, Y. Lu, C. D. Amos, A. Manthiram and J. B. Goodenough, Role of Oxygen Vacancies on the Performance of $\text{Li}[\text{Ni}_{0.5-x}\text{Mn}_{1.5+x}]\text{O}_4$ ($x=0, 0.05, \text{ and } 0.08$) Spinel Cathodes for Lithium-Ion Batteries. *Chem. Mater.* **2012**, 24, 3101.

14. E. McCalla and J. R. Dahn, The spinel and cubic rocksalt solid-solutions in the Li-Mn-Ni oxide pseudo-ternary system. *Solid State Ionics* **2013**, 242, 1.

15. A. Manthiram, K. Chemelewski and E-S Lee, A perspective on the high-voltage $\text{LiMn}_{1.5}\text{Ni}_{0.5}\text{O}_4$ spinel cathode for lithium-ion batteries. *Energy Environ. Sci.* **2014**, 7, 1339.

16 J. Xiao, X. Chen, P.V. Sushko, M.L. Sushko, L. Kovarik, J. Feng, Z.Deng, J.Zheng, G.L. Graff, Z. Nie, D. Choi, J. Liu , J.-G. Zhang, and M. S. Whittingham, High-Performance $\text{LiNi}_{0.5}\text{Mn}_{1.5}\text{O}_4$ Spinel Controlled by Mn^{3+} Concentration and Site Disorder. *Adv. Mater.* **2012**, 24, 2109

17. K. Xu, Nonaqueous Liquid Electrolytes for Lithium-Based Rechargeable Batteries. *Chem. Rev.* **2004**, 104, 4303.

18. L. Yang, B. Ravdel and B. Lucht, Electrochem., Electrolyte Reactions with the Surface of High Voltage $\text{LiNi}_{0.5}\text{Mn}_{1.5}\text{O}_4$ Cathodes for Lithium-Ion Batteries. *Solid-State Lett.* **2010** 13, A95.

19 Choi, N.-S.; Yeon, J.-T.; Lee, Y.-W.; Han, J.-G.; Lee, K. T.; Kim, S.-S., Degradation of spinel lithium manganese oxides by low oxidation durability of LiPF_6 -based electrolyte at 60° C. *Solid State Ionics* **2012**, 219, 41.

20. Jang, D. H.; Oh, S. M., Electrolyte Effects on Spinel Dissolution and Cathodic Capacity Losses in 4 V $\text{Li}/\text{Li}_x\text{Mn}_2\text{O}_4$ Rechargeable Cells. *Journal of The Electrochemical Society* **1997**, 144 (10), 3342-3348.

21. V. Borgel, E. Markevich, D. Aurbach, G. Semrau and M. Schmidt, On the application of ionic liquids for rechargeable Li batteries: High voltage systems. *J. Power Sources* **2009**, 189, 331.
22. Y. A. Lebdeh and I. Davidson, High-Voltage Electrolytes Based on Adiponitrile for Li-Ion Batteries. *J. Electrochem. Soc.* **2009**, 156, A60.
23. K. Xu, S. Zhang, T. R. Jow, W. Xu and C. A. Angell, LiBOB as Additive in LiPF₆-Based Lithium Ion Electrolytes. *Electrochem. Solid-State Lett.* **2005**, 8, A365.
24. N.-S. Choi, K. H. Yew, H. Kim, S.-S. Kim and W.-U. Choi, Surface layer formed on silicon thin-film electrode in lithium bis(oxalato) borate-based electrolyte. *J. Power Sources* **2007**, 172, 404.
25. K. Xu, S. S. Zhang, U. Lee, J. L. Allen and T. R. Jow, LiBOB: Is it an alternative salt for lithium ion chemistry? *J. Power Sources* **2005**, 146, 79.
26. K. Xu and C. A. Angell, *J. Electrochem. Soc.*, 2002, 149, A920. 7 N. Shao, X.-G. Sun, S. Dai and D. Jiang, Oxidation Potentials of Functionalized Sulfone Solvents for High-Voltage Li-Ion Batteries: A Computational Study. *J. Phys. Chem. B*, **2012**, 116, 3235.
27. Z. Zhang, L. Hu, H. Wu, W. Weng, M. Koh, P. C. Redfern, L. A. Curtiss and K. Amine, *Energy Environ. Sci.* **2013**, 6, 1806.
28. Z.N. Wang, Y.J. Cai, Z.H. Wang, S.M. Chen, X.M. Lu, S.J. Zhang, Vinyl-functionalized imidazolium ionic liquids as new electrolyte additives for high-voltage Li-ion batteries. *J Solid State Electrochem* **2013**, 17, 2839.
29. N.-S. Choi, Z. Chen, S. A. Freunberger, X. Ji, Y.-K. Sun, K. Amine, G. Yushin, L. F. Nazar, J. Cho and P. G. Bruce, Challenges Facing Lithium Batteries and Electrical Double-Layer Capacitors. *Angew. Chem. Int. Ed.* **2012**, 51, 9994.
30. I. H. Cho, S.-S. Kim, S. C. Shin and N.-S. Choi, Electrochem., Effect of SEI on Capacity Losses of Spinel Lithium Manganese Oxide/Graphite Batteries Stored at 60°C. *Solid-State Lett.* **2010**, 13, A168.
31. R. J. Gummow and A. de Kock, Improved capacity retention in rechargeable 4 V lithium/lithium-

manganese oxide (spinel) cells. *Solid State Ionics* **1994**, 69, 59.

32. E. Wang, D. Ofer, W. Bowden, N. Itchev, R. Moses and K. Brandt, Stability of Lithium Ion Spinel Cells III. Improved Life of Charged Cells. *J. Electrochem. Soc.* **2000**, 147, 4023.

33. H. Tsunekawa, S. Tanimoto, R. Marubayashi, M. Fujita, K. Kifune and M. Sano, Capacity Fading of Graphite Electrodes Due to the Deposition of Manganese Ions on Them in Li-Ion Batteries. *J. Electrochem. Soc.* **2002**, 149, A1326.

34. N.-S. Choi, J.-T. Yeon, Y.-W. Lee, J.-G. Han, K. T. Lee and S.-S. Kim, Degradation of spinel lithium manganese oxides by low oxidation durability of LiPF₆-based electrolyte at 60 °C. *Solid State Ionics* **2012**, 219, 41.

35. S. Brutti, V. Gentili, P. Reale, L. Carbone and S. Panero, Mitigation of the irreversible capacity and electrolyte decomposition in a LiNi_{0.5}Mn_{1.5}O₄/nano-TiO₂ Li-ion battery. *J. Power Sources* **2011**, 196, 9792.

36. L. Baggetto, R. R. Unocic, N. J. Dudney and G. M. Veith, Fabrication and characterization of LiMnNiO sputtered thin film high voltage cathodes for Li-ion batteries. *J. Power Sources*, **2012**, 211, 108.

37. S. K. Martha, E. Markevich, V. Burgel, G. Salitra, E. Zinigrad, B. Markovsky, H. Sclar, Z. Pramovich, O. Heik, D. Aurbach, I. Exnar, H. Buqa, T. Drezen, G. Semrau, M. Schmidt, D. Kovacheva and N. Saliyski, A short review on surface chemical aspects of Li batteries: A key for a good performance. *J. Power Sources* **2009**, 189, 288.

38. S.-Y. Ha, J.-G. Han, Y.-M. Song, M.-J. Chun, S.-I. Han, W.-C. Shin and N.-S. Choi, Using a lithium bis(oxalato) borate additive to improve electrochemical performance of high-voltage spinel LiNi_{0.5}Mn_{1.5}O₄ cathodes at 60 degrees C. *Electrochim. Acta*, **2013**, 104, 170.

39. N. P. W. Pieczonka, L. Yang, M. P. Balogh, B. R. Powell, K. Chemelewski, A. Manthiram, S. A. Krachkovskiy, G. R. Goward, M. Liu and J.-H. Kim, Impact of Lithium Bis(oxalate)borate Electrolyte Additive on the Performance of High-Voltage. *J. Phys. Chem. C*, **2013**, 117, 22603.

40. H. Duncan, Y. Abu-Lebdeh and I. J. Davidson, Study of the Cathode-Electrolyte Interface of

LiMn_{1.5}Ni_{0.5}O₄ Synthesized by a Sol-Gel Method for Li-Ion Batteries. *J. Electrochem. Soc.* 2010, 157, A528.

41. S.A. Delp, J.L. Allen, T. R. Jow, Investigation of Electrolyte Additives with LiNi_{0.5}Mn_{1.5}O₄/Graphite Cells at High Temperature. *ECS Transactions* **2014**, 58 (48) 111

42. C. Arbizzani, F.D. Giorgio, L. Porcarelli, M. Mastragostino, V. Khomenko, V. Barsukov, D. Bresser, S. Passerini, Use of non-conventional electrolyte salt and additives in high-voltage graphite/LiNi_{0.4}Mn_{1.6}O₄ batteries. *Journal of Power Sources* **2013**, 238, 17.

43. Y.-S. Kang, T. Yoon, S.S. Lee, J. Mun, M.S. Park, J.-H. Park, S.-G. Doo, I.-Y. Song, S.M. Oh, 1,3,5-Trihydroxybenzene as a film-forming additive for high-voltage positive electrode. *Electrochemistry Communications* **2013**, 27, 26.

44. G. Yan, X. Li, Z. Wang, H. Guo, X Xiong, Beneficial effects of 1-propylphosphonic acid cyclic anhydride as an electrolyte additive on the electrochemical properties of LiNi_{0.5}Mn_{1.5}O₄ cathode material. *Journal of Power Sources* **2014**, 263, 231.

45. A. Abouimrane, S. A. Odom, H Tavassol, M. V. Schulmerich, H. Wu, R. Bhargava, A. A. Gewirth, J. S. Moore, K A, 3-Hexylthiophene as a Stabilizing Additive for High Voltage Cathodes in Lithium-Ion Batteries. *Journal of The Electrochemical Society* **2013**, 160, A268 .

46. W. Huang, L. Xing, Y. Wang, M. Xu, W. Li, F. Xie, S. Xia, 4-(Trifluoromethyl)-benzotrile: A novel electrolyte additive for lithium nickel manganese oxide cathode of high voltage lithium ion battery. *Journal of Power Sources* **2014**, 267, 560.

47. E. Markevich, G. Salitra, K. Fridman, R. Sharabi, G. Gershinsky, A. Garsuch, G. Semrau, M. A. Schmidt, D. Aurbach, Fluoroethylene Carbonate as an Important Component in Electrolyte Solutions for High-Voltage Lithium Batteries: Role of Surface Chemistry on the Cathode. *Langmuir* **2014**, 30, 7414.

48. H.W. Rollins, M. K. Harrup, E. J. Dufek, D. K. Jamison, S. V. Sazhin, K. L. Gering, D. L. Daubaras, Fluorinated phosphazene co-solvents for improved thermal and safety performance in lithium-ion battery electrolytes. *Journal of Power Sources* **2014**, 263, 66.

49. H. Bouayad, Z. Wang, N. Dupré, R. Dedryvère, D. Foix, S. Franger, J.-F. Martin, L. Boutafa, S. Patoux, D. Gonbeau, and D. Guyomard, Improvement of Electrode/Electrolyte Interfaces in High-Voltage Spinel Lithium-Ion Batteries by Using Glutaric Anhydride as Electrolyte Additive. *J. Phys. Chem. C* **2014**, 118, 4634.
50. Z.D. Li, Y.C. Zhang, H.F. Xiang, X.H. Ma, Q.F. Yuan, Q.S. Wang, C.H. Chen, Trimethyl phosphite as an electrolyte additive for high-voltage lithium-ion batteries using lithium-rich layered oxide cathode. *Journal of Power Sources* **2013**, 240, 471.
51. M. Xu, Y. Liu, B. Li, W. Li, X.Li, S. Hu, Tris (pentafluorophenyl) phosphine: An electrolyte additive for high voltage Li-ion batteries. *Electrochemistry Communications* **2012**, 18, 123.
52. H. Rong, M. Xu, L. Xing, W. Li, Enhanced cyclability of LiNi_{0.5}Mn_{1.5}O₄ cathode in carbonate based electrolyte with incorporation of tris(trimethylsilyl)phosphate (TMSP). *Journal of Power Sources* **2014**, 261, 148.
53. G. Yan, X. Li, Z. Wang, H. Guo, C. Wang, Tris(trimethylsilyl)phosphate: A film-forming additive for high voltage cathode material in lithium-ion batteries. *Journal of Power Sources* **2014**, 248, 1306.
54. A. V. Cresce and K. Xu, Electrolyte Additive in Support of 5 V Li Ion Chemistry. *J. Electrochem. Soc.* **2011**, 158, A337.
55. Y.-M. Song, J.-G. Han, S. Park, K.T. Lee, N.-S. Choi, A multifunctional phosphite-containing electrolyte for 5 V-class LiNi_{0.5}Mn_{1.5}O₄ cathodes with superior electrochemical performance. *J. Mater. Chem. A*, **2014**, 2, 9506.
56. K. Tasaki, A. Goldberg, J.-J. Lian, M. Walker, A. Timmons and S. J. Harris, Solubility of Lithium Salts Formed on the Lithium-Ion Battery Negative Electrode Surface in Organic Solvents. *J. Electrochem. Soc.* **2009**, 156, A1019.
57. N.-S. Choi, Y. Yao, Y. Cui and J. Cho, One dimensional Si/Sn - based nanowires and nanotubes for lithium-ion energy storage materials. *J. Mater. Chem.* **2011**, 21, 9825.
58. M.-J. Chun, H. Park, S. Park and N.-S. Choi, Bicontinuous structured silicon anode exhibiting stable cycling performance at elevated temperature. *RSC Adv.* **2013**, 3, 21320.

59. H.-B. Han, S.-S. Zhou, D.-J. Zhang, S.-W. Feng, L.-F. Li, K. Liu, W.-F. Feng, J. Nie, H. Li, X.-J. Huang, M. Armand and Z.-B. Zhou, Electrolyte Additive in Support of 5 V Li Ion Chemistry Lithium bis(fluorosulfonyl)imide (LiFSI) as conducting salt for nonaqueous liquid electrolytes for lithium-ion batteries: Physicochemical and electrochemical properties. *J. Power Sources*, **2011**, 196, 3623.
60. C. L. Champion, W. Li and B. L. Lucht, Thermal decomposition of LiPF₆-based electrolytes for lithium-ion batteries. *J. Electrochem. Soc.* **2005**, 152, A2327.
61. S. Dalavi, M. Xu, B. Ravdel, L. Zhou and B. L. Lucht, Nonflammable Electrolytes for Lithium-Ion Batteries Containing Dimethyl Methylphosphonate. *J. Electrochem. Soc.* **2010**, 157, A1113.
62. S.-K. Jeong, M. Inaba, R. Mogi, Y. Iriyama, T. Abe and Z. Ogumi, Surface film formation on a graphite negative electrode in lithium-ion batteries: Atomic force microscopy study on the effects of film-forming additives in propylene carbonate solutions. *Langmuir*, **2001**, 17, 8281.
63. M. Itagaki, S. Yotsuda, N. Kobari, K. Watanabe, S. Kinoshita and M. Ue, Electrochemical impedance of electrolyte/electrode interfaces of lithium-ion rechargeable batteries - Effects of additives to the electrolyte on negative electrode. *Electrochim. Acta*, **2006**, 51, 1629.
64. X.-P. Gao and H.-X. Yang, Multi-electron reaction materials for high energy density batteries. *Energy Environ. Sci.* **2010**, 3, 174–189